

Reconstructing Stieltjes functions from their approximate values: a search for a needle in a hay stack

Yury Grabovsky

February 12, 2021

Abstract

Material response of passive media to external influences is described by complex analytic functions of frequency that can always be written in terms of Stieltjes functions—a special class of analytic functions mapping complex upper half-plane into itself. Reconstructing such functions from their experimentally measured values at specific frequencies is one of the central problems that we address in this paper. A definitive reconstruction algorithm that produces a certificate of optimality as well as a graphical representation of the uncertainty of reconstruction is proposed. Its effectiveness is demonstrated in the context of the electrochemical impedance spectroscopy.

Contents

1	Introduction	2
2	Preliminaries and background	4
2.1	The Nevanlinna-Pick theorem for Stieltjes functions	4
2.2	Bounds on Stieltjes function values	5
2.3	Interpolation	8
2.4	The least squares problem	15
2.5	Analytic structure of the boundary of $V(z)$	18
3	A needle in a haystack	20
4	The least squares algorithm	24
5	Direct computation of spectral measure	29
6	Case study: Electrochemical impedance spectroscopy	31

1 Introduction

Three fundamental physical principles: causality, time-invariance, and passivity are responsible for the ubiquity of Stieltjes functions in physics and engineering. *Stieltjes class* refers to a special class of complex analytic functions that describe the response of linear media or devices to external influences. If $E(t)$ denotes such an influence, and $J(t)$ the response, then the causal, linear, time-invariant dependence of $J(t)$ on $E(t)$ could be formally written (without regard to the function spaces to which $E(t)$ and $J(t)$ may belong) as

$$J(t) = \gamma_0 E(t) + \int_{-\infty}^t a(t - \tau) E(\tau) d\tau. \quad (1.1)$$

This formula shows that $J(t)$ may depend on all past values $E(\tau)$, $\tau \leq t$, where the factor $a(t - \tau)$ attenuating each such value depends on how far in the past it has occurred. Typically, the memory kernel $a(s)$ decays exponentially, as $s \rightarrow \infty$. Due to the resemblance of the integral in (1.1) to a convolution, it is convenient to extend the memory kernel $a(s)$ to negative values of s by zero

$$a_0(s) = \begin{cases} a(s), & s \geq 0, \\ 0, & s < 0, \end{cases}$$

and rewrite (1.1) as a convolution

$$J(t) = \gamma_0 E(t) + \int_{-\infty}^{\infty} a_0(t - \tau) E(\tau) d\tau. \quad (1.2)$$

Assuming now that $a_0 \in L^1(\mathbb{R})$ and $\{E, J\} \subset L^2(\mathbb{R})$ we can take the Fourier transform of (1.2):

$$\widehat{J}(\omega) = (\gamma_0 + \widehat{a}_0(\omega)) \widehat{E}(\omega). \quad (1.3)$$

Two different definitions of the Fourier transform are common in physics, depending on the representation of the input $E(t)$ as a superposition of “elementary harmonics”. In signal processing the elementary harmonics are functions $e^{i\omega t}$, leading to the representation

$$E(t) = \frac{1}{2\pi} \int_{-\infty}^{\infty} \widehat{E}(\omega) e^{i\omega t} d\omega, \quad \widehat{E}(\omega) = \int_{-\infty}^{\infty} E(t) e^{-i\omega t} dt.$$

In electromagnetics the elementary harmonics are the plane waves $e^{i(\mathbf{k} \cdot \mathbf{x} - \omega t)} = E_0(\mathbf{x}) e^{-i\omega t}$. In this case one uses

$$E(t) = \frac{1}{2\pi} \int_{-\infty}^{\infty} \widehat{E}(\omega) e^{-i\omega t} d\omega, \quad \widehat{E}(\omega) = \int_{-\infty}^{\infty} E(t) e^{i\omega t} dt.$$

In the former case causality ($a_0(s) = 0$, when $s < 0$) implies that $b(\omega) = \gamma_0 + \widehat{a}_0(\omega)$ is analytic in the lower half-plane of the complex ω -plane, in the latter, $b(\omega)$ is analytic in the upper half-plane. In each case the fact that the memory kernel $a(s)$ is a real-valued function implies that $b(\omega)$ has the symmetry

$$\overline{b(\omega)} = b(-\overline{\omega}). \quad (1.4)$$

The passivity principle, that says that the medium can only absorb or dissipate energy is a much more delicate condition leading to the nonnegativity of the real or imaginary parts of functions related to $b(\omega)$. In one way or another in each and every application the description of the passive, causal, time-invariant media response can be formulated in terms of functions from the Stieltjes class \mathfrak{S} .

Definition 1.1. *We say that a complex function f analytic in $\mathbb{C} \setminus \mathbb{R}_+$ belongs to the Stieltjes class \mathfrak{S} if it is either a nonnegative real constant or has the following three properties.*

- (i) $\mathfrak{Im}(f(z)) > 0$ for all $z \in \mathbb{C}$ with $\mathfrak{Im}(z) > 0$;
- (ii) $f(x) > 0$ for all $x < 0$;
- (iii) $\overline{f(z)} = f(\bar{z})$.

For example, the complex electromagnetic permittivity $\varepsilon(\omega)$ of dielectrics can be written as $\varepsilon(\omega) = f(\omega^2)$, where $f \in \mathfrak{S}$ and $\mathfrak{Im}(\omega) > 0$ [31, 20]. Both the complex impedance and admittance functions $Z(\omega)$ and $Y(\omega)$, respectively, of electric circuits made of resistors, capacitors and inductive coils can be written as $Z(\omega) = i\omega f(\omega^2)$, where $f \in \mathfrak{S}$ and $\mathfrak{Im}(\omega) < 0$, [11]. In high energy physics it is the energy (or momentum) that plays the role of the complex variable and the diagonal components (in any basis) of the scattering S-matrix are the Stieltjes functions [36, 35, 7]. In the theory of binary conducting composites the dependence of the effective conductivity σ^* of the composite on the ratio $h = \sigma_2/\sigma_1$ of the conductivities of two constituents is also expressible in terms of Stieltjes functions, [6, 39, 25, 33]

$$\frac{\sigma^*}{\sigma_1} = 1 + \left(1 - \frac{1}{h}\right) f\left(-\frac{1}{h}\right), \quad f \in \mathfrak{S}.$$

There are many other applications (see e.g. [41]), where the models are linear and the three fundamental physical principles of causality, time-invariance, and passivity lead to functions from the Stieltjes class \mathfrak{S} .

In this paper we consider the central problem of the theory of Stieltjes functions that arises in all applications: the identification of $f \in \mathfrak{S}$ from a finite number n of measurements at the n distinct points $\{z_1, \dots, z_n\} \subset \mathbb{H}_+$. The analyticity of $f \in \mathfrak{S}$ places constraints on the values $f(z_j)$. It turns out that the constraints are so delicate that even if one truncates the infinite decimal representations of the values $w_j = f(z_j)$ in order to store them as floating point numbers in a computer, one violates these constraints when $n \geq 15$. In most applications the values $w_j = f(z_j)$ are obtained through experimental measurements where the noise level is much larger than the round-off errors in floating point arithmetic. In view of these considerations the central problem is not the recovery of $f \in \mathfrak{S}$ from its exact values $w_j = f(z_j)$, but rather the minimization of the sum of squares

$$\Sigma(\mathbf{w}, \mathbf{z}) = \inf_{f \in \mathfrak{S}} \sum_{j=1}^n |f(z_j) - w_j|^2 \tag{1.5}$$

for a given set of noisy measurements $\mathbf{w} \in \mathbb{C}^n$. The problem of solving (1.5) bears only superficial resemblance to the classical linear least squares problem. The main difficulty is that the Stieltjes class \mathfrak{S} is not a vector space, but a convex cone.

In various guises this problem has been studied continuously for almost a century. Yet, so far, no definitive algorithm has emerged, and new algorithms and new papers on the subject continue to appear with unerring regularity (e.g. [8, 34, 38, 46], to give a taste). In this paper we propose such a definitive algorithm that is aimed to settle the question once and for all. The algorithm comes with a “certificate of optimality” based on the work of I. Caprini [12, 13, 14, 15].

The main issue lies in intricacies of the geometry of the *feasible set*

$$V(\mathbf{z}) = \{(f(z_1) \dots, f(z_n)) \in \mathbb{C}^n : f \in \mathfrak{S}\}, \quad \mathbf{z} = (z_1, \dots, z_n), \quad (1.6)$$

which is known to be a closed convex cone in \mathbb{C}^n with non-empty interior. In practice, however, $V(\mathbf{z})$ is massively dimensionally degenerate, shaped very much like a needle. Even for modest values of n the smallest thickness of $V(\mathbf{z})$ is well below double precision floating point arithmetic. The proposed algorithm harnesses this dimensional degeneracy and turns it from a curse into a blessing. The algorithm produces not only the solution $f \in \mathfrak{S}$ of (1.5), but also shows the uncertainty associated with the given data. Typical for analytic continuation problems the uncertainty balloons and explodes once one goes outside of the frequency range containing the measurements [19, 44, 4, 26, 27].

The paper begins with the recollection of known results about Stieltjes functions in Section 2. In Section 3 we show that the feasible set $V(\mathbf{z})$ is shaped like a needle or maybe like a sword. (Our language has a very limited vocabulary for three-dimensional shapes.) In Section 4 we describe the algorithm. The performance of the algorithm is demonstrated in Section 6 in the context of electrochemistry, where the processes of corrosion and electrolysis that occur in batteries and in many other natural and man-made systems can be modeled by Voigt circuits—electrical circuits made only of resistors and capacitors [43, 1, 2]. The electrochemical impedance spectrum (EIS) function $Z(\omega)$ can then be written as $f(-i\omega)$ for some $f \in \mathfrak{S}$. Thus, the values $Z_j = f(-i\omega_j)$, $j = 1, \dots, n$ can be measured experimentally at particular frequencies $\omega_1, \dots, \omega_n$. Our algorithm takes noisy measurements of Z_1, \dots, Z_n as the input and generates physically admissible EIS function $Z(\omega)$, representing it both numerically and as the explicit complex impedance function of a small Voigt circuit. It also displays the certificate of optimality as well as the uncertainty of reconstruction of the EIS function for the specific data. Figure 6 shows the typical graphical output of the algorithm.

2 Preliminaries and background

2.1 The Nevanlinna-Pick theorem for Stieltjes functions

There are two related definitions of the Stieltjes class \mathfrak{S} differing by the choice of the domain of analyticity. In this paper a Stieltjes function, described in Definition 1.1, is analytic in $\mathbb{C} \setminus \mathbb{R}_+$ (the complex plane cut along the positive real line). We recall two equivalent characterizations of \mathfrak{S} . One exhibits the centrality of property (i) in Definition 1.1, which is an expression of passivity in frequency domain. The other gives an explicit representation of all Stieltjes functions. Let $\mathbb{H}_+ = \{z \in \mathbb{C} : \Im(z) > 0\}$ denote the complex upper half-plane.

Definition 2.1. We say that $f(z)$ analytic in \mathbb{H}_+ is a Nevanlinna function if it is either a real constant function or $\Im m(f(z)) > 0$ for all $z \in \mathbb{H}_+$.

THEOREM 2.2. $f \in \mathfrak{S}$ if and only if both f and $z \mapsto zf(z)$ are Nevanlinna functions.

As a corollary we see that the Stieltjes class has an involutive symmetry

$$f(z) \mapsto -\frac{1}{zf(z)}. \quad (2.1)$$

The second characterization of \mathfrak{S} is more explicit.

THEOREM 2.3 (Stieltjes). $f \in \mathfrak{S}$ if and only if there exists $\gamma \geq 0$ and a positive Radon measure σ on $[0, +\infty)$, such that

$$f(z) = \gamma + \int_0^\infty \frac{d\sigma(t)}{t-z}, \quad \int_0^\infty \frac{d\sigma(t)}{1+t} < +\infty. \quad (2.2)$$

The proof of both theorems can be found in [30]. We remark that given $f \in \mathfrak{S}$ we have

$$\gamma = \lim_{z \rightarrow \infty} f(z), \quad \sigma(x) = \frac{1}{\pi} \lim_{y \rightarrow 0^+} \Im m f(x + iy), \quad (2.3)$$

where the second limit above is understood in the sense of distributions.

Our goal is the recovery of a Stieltjes function f from its possibly imperfectly measured values $f(z_1), \dots, f(z_n)$ at distinct points $\{z_1, \dots, z_n\} \subset \mathbb{H}_+$. In this regard we recall a well-known Nevanlinna-Pick theorem that gives a criterion for $\mathbf{w} \in \mathbb{C}^n$ to lie in the feasible set $V(\mathbf{z})$, given by (1.6).

THEOREM 2.4 (Nevanlinna-Pick). Let $\{z_1, \dots, z_n\} \subset \mathbb{H}_+$ be all distinct and $\mathbf{w} \in \mathbb{C}^n$. Then $\mathbf{w} \in V(\mathbf{z})$ if and only if the Nevanlinna-Pick matrices $\mathbf{N}(\mathbf{w})$ and $\mathbf{P}(\mathbf{w})$ are nonnegative definite, where

$$N_{jk} = \frac{w_j - \overline{w_k}}{z_j - \overline{z_k}}, \quad P_{jk} = \frac{z_j w_j - \overline{z_k w_k}}{z_j - \overline{z_k}}. \quad (2.4)$$

Moreover, if $\mathbf{w} \in \partial V(\mathbf{z})$, so that either $\text{rank}(\mathbf{N}(\mathbf{w})) < n$ or $\text{rank}(\mathbf{P}(\mathbf{w})) < n$, then there is a unique rational function $f \in \mathfrak{S}$, such that $w_j = f(z_j)$, $j = 1, \dots, n$.

The proof can be found in [30].

2.2 Bounds on Stieltjes function values

The question we want to address now is about the freedom one has for the value $w = f(z)$, provided $f \in \mathfrak{S}$ and satisfies $f(z_j) = w_j$, $j = 1, \dots, n$. This freedom is represented by the admissible set of values

$$\mathcal{A}(z; \mathbf{z}, \mathbf{w}) = \{f(z) : f \in \mathfrak{S}, f(z_j) = w_j, j = 1, \dots, n\}. \quad (2.5)$$

Such admissible sets are well-understood and widely used in the context of effective properties of composite materials [25, 23, 24, 37, 18]. Our analysis is inspired by the one in [40] and

reaches somewhat similar conclusions. However, it is based on Theorem 2.4 rather than the explicit representation of Stieltjes functions from Theorem 2.3, used in prior work.

Let us assume that the data \mathbf{w} lies in the interior of $V(\mathbf{z})$. By Theorem 2.4 the matrices $\mathbf{N}(\mathbf{z}, \mathbf{w})$ and $\mathbf{P}(\mathbf{z}, \mathbf{w})$, given by (2.4), are positive definite. Then, by the Sylvester criterion we obtain that the $\mathbf{N}([\mathbf{z}, z], [\mathbf{w}, w])$ and $\mathbf{P}([\mathbf{z}, z], [\mathbf{w}, w])$ matrices corresponding to the extended data $([\mathbf{z}, z], [\mathbf{w}, w])$ are positive definite if and only if

$$\det \mathbf{N}([\mathbf{z}, z], [\mathbf{w}, w]) > 0, \quad \det \mathbf{P}([\mathbf{z}, z], [\mathbf{w}, w]) > 0. \quad (2.6)$$

We can make inequalities (2.6) explicit, since the determinants above are quadratic functions of w . Expanding the determinants with respect to the last column and the last row, so that w enters explicitly we obtain

$$\det \mathbf{N}([\mathbf{z}, z], [\mathbf{w}, w]) = \frac{\Im(w)}{\Im(z)} \det \mathbf{N}(\mathbf{z}, \mathbf{w}) - \alpha |w|^2 + 2\Re(aw) - \beta,$$

where

$$\alpha = (\text{cof}(\mathbf{N})\boldsymbol{\xi}(z), \boldsymbol{\xi}(z)), \quad a = (\text{cof}(\mathbf{N})\boldsymbol{\xi}(z), \boldsymbol{\eta}(z)), \quad \beta = (\text{cof}(\mathbf{N})\boldsymbol{\eta}(z), \boldsymbol{\eta}(z)),$$

and

$$\xi_k(z) = \frac{1}{z - \bar{z}_k}, \quad \eta_k(z) = \frac{\bar{w}_k}{z - \bar{z}_k}, \quad k = 1, \dots, n.$$

We conclude that $\det \mathbf{N}([\mathbf{z}, z], [\mathbf{w}, w]) > 0$ if and only if $|w - w^{(N)}(z)| < r_N(z)$, where

$$w^{(N)}(z) = \frac{\bar{a}}{\alpha} + i \frac{\det \mathbf{N}(\mathbf{w})}{2\alpha \Im(z)}, \quad r_N(z)^2 = |w^{(N)}(z)|^2 - \frac{\beta}{\alpha}. \quad (2.7)$$

A similar analysis for the \mathbf{P} -matrix gives $|w - w^{(P)}(z)| < r_P(z)$, where

$$w^{(P)}(z) = \frac{\bar{a}'}{\alpha'} + i \frac{\bar{z} \det \mathbf{P}(\mathbf{w})}{2\alpha' \Im(z)}, \quad r_P(z)^2 = |w^{(P)}(z)|^2 - \frac{\beta'}{\alpha'}, \quad (2.8)$$

and

$$\alpha' = (\text{cof}(\mathbf{P})\boldsymbol{\xi}'(z), \boldsymbol{\xi}'(z)), \quad a' = (\text{cof}(\mathbf{P})\boldsymbol{\xi}'(z), \boldsymbol{\eta}'(z)), \quad \beta' = (\text{cof}(\mathbf{P})\boldsymbol{\eta}'(z), \boldsymbol{\eta}'(z)),$$

$$\boldsymbol{\xi}'(z) = z\boldsymbol{\xi}(z), \quad \boldsymbol{\eta}'(z) = z\boldsymbol{\eta}(z) - \bar{\mathbf{w}}.$$

Let us now estimate $r_N(z)$. (The estimate for $r_P(z)$ would be fully analogous.) The key observation is the inequality between α , β and a : $|a|^2 \leq \alpha\beta$. Then

$$r_N(z)^2 = \frac{|a|^2 - \alpha\beta}{\alpha^2} + \rho^2 - \frac{2\Im(a)\rho}{\alpha} \leq 2\rho \left(\rho - \frac{\Im(a)}{\alpha} \right) = 2\rho \Im(w^{(N)}(z)), \quad \rho = \frac{\det \mathbf{N}(\mathbf{w})}{2\alpha \Im(z)}.$$

Thus, we have obtained the estimate

$$r_N(z)^2 \leq \frac{\Im(w^{(N)}(z))}{\Im(z)} (\mathbf{N}(\mathbf{w})^{-T} \boldsymbol{\xi}(z), \boldsymbol{\xi}(z))^{-1}. \quad (2.9)$$

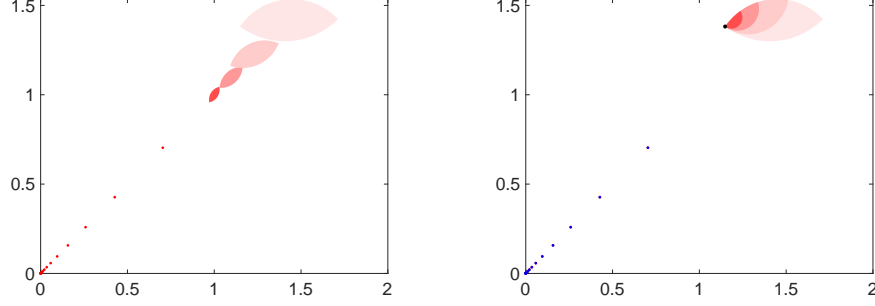


Figure 1: Dependence of the admissible set $\mathcal{A}(z; \mathbf{z}, \mathbf{w})$ on the location of z , relative to the data z_j .

A similar calculation for the \mathbf{P} matrix gives the estimate

$$r_P(z)^2 \leq \frac{\Im(zw^{(P)}(z))}{\Im(z)} (\mathbf{P}(\mathbf{w})^{-T} \boldsymbol{\xi}'(z), \boldsymbol{\xi}'(z))^{-1}. \quad (2.10)$$

The main feature of matrices $\mathbf{N}(\mathbf{w})$ and $\mathbf{P}(\mathbf{w})$ is the exponential decay of their eigenvalues due to their rank two displacement structure [5]:

$$\mathbf{D}(z)\mathbf{N}(\mathbf{w}) - \mathbf{N}(\mathbf{w})\mathbf{D}(z)^* = \mathbf{w} \otimes \mathbf{1} - \mathbf{1} \otimes \overline{\mathbf{w}}, \quad (2.11)$$

$$\mathbf{D}(z)\mathbf{P}(\mathbf{w}) - \mathbf{P}(\mathbf{w})\mathbf{D}(z)^* = \mathbf{D}(z)\mathbf{w} \otimes \mathbf{1} - \mathbf{1} \otimes \mathbf{D}(\overline{z})\overline{\mathbf{w}}, \quad (2.12)$$

where $\mathbf{D}(z)$ is a diagonal matrix with numbers z_j on the main diagonal and $\mathbf{1}$ is a vector of ones.

If the vector $\boldsymbol{\xi}(z)$ has a substantial projection onto the space spanned by the eigenvectors of $\mathbf{N}(\mathbf{w})$ and $\mathbf{P}(\mathbf{w})$ with exponentially small eigenvalues, then $(\mathbf{N}(\mathbf{w})^{-T} \boldsymbol{\xi}(z), \boldsymbol{\xi}(z))$ and $(\mathbf{P}(\mathbf{w})^{-T} \boldsymbol{\xi}'(z), \boldsymbol{\xi}'(z))$ will be exponentially large (as functions of n). This shows that $r_N(z)$ and $r_P(z)$ can easily become exponentially small even for relatively small values of n . In fact, $r_N(z) = 0$ or $r_P(z) = 0$ (or both) whenever $\mathbf{w} \in \partial V(\mathbf{z})$. This may lead one to think that fixing more than 15–20 values of a Stieltjes function determines it for all practical intents and purposes. Those who have tried to develop extrapolation algorithms for analytic functions know very well just how false this is in practice. The explanation lies in the geometry of $V(\mathbf{z})$. Formally, $V(\mathbf{z})$ is a closed convex cone in \mathbb{C}^n with non-empty interior. In practice, its geometry resembles that of a thin knife blade, rather than a party hat, so that very small random perturbations of points in the interior of $V(\mathbf{z})$ will throw them outside. In other words, no matter where the point \mathbf{w} is in $V(\mathbf{z})$, it is never far from $\partial V(\mathbf{z})$, where, as we have just observed, the region of admissible values $\mathcal{A}(z; \mathbf{z}, \mathbf{w})$ degenerates to a point. What is somewhat counter-intuitive is that for points \mathbf{w} in the interior of $V(\mathbf{z})$ the set $\mathcal{A}(z; \mathbf{z}, \mathbf{w})$ can be rather large, depending on the location of z relative to points z_j . The left panel of Figure 1 illustrates this effect in the simple example

$$z_j = ie^{0.01+j}, \quad w_j = f(z_j), \quad j = 0, 1, \dots, 19, \quad f(z) = \frac{1}{\sqrt{-z}}. \quad (2.13)$$

We see how the shaded lens-shaped regions grow in size as the point z , taking values $i/2$, $i/2.4$, $i/3$, and $i/4$ moves “away” from the data z_j , given in (2.13). Our discussion also shows that if we move \mathbf{w} from the interior of $V(\mathbf{z})$ to its boundary the admissible set will shrink to a point. The right panel of Figure 1 illustrates this effect when we move from \mathbf{w} , given in (2.13), which lies in the interior of $V(\mathbf{z})$, to $\partial V(\mathbf{z})$ along any random direction \mathbf{u} , which we have chosen (arbitrarily) to have all components equal to -1 . The corresponding point $\tilde{\mathbf{w}} \in \partial V(\mathbf{z})$ satisfies

$$|\mathbf{w} - \tilde{\mathbf{w}}|/|\mathbf{w}| < 10^{-4},$$

as we have verified numerically. In the right panel of Figure 1 we plotted the original points w_j in red and the perturbed points \tilde{w}_j in blue, except one cannot see a difference between them in the figure. The set $\mathcal{A}(z; \mathbf{z}, \tilde{\mathbf{w}})$ degenerates to a point shown in black, while the sets $\mathcal{A}_t = \mathcal{A}(z; \mathbf{z}, t\tilde{\mathbf{w}} + (1-t)\mathbf{w})$ for three intermediate values of t are shown by progressively darker shading. The values we have chosen are $t_1 = 1 - 2 \cdot 10^{-5}$, $t_2 = 1 - 7 \cdot 10^{-6}$, and $t_3 = 1 - 3 \cdot 10^{-6}$. This indicates that if we move uniformly from $\mathbf{w} \in V(\mathbf{z})$ to $\tilde{\mathbf{w}} \in \partial V(\mathbf{z})$, the admissible sets \mathcal{A}_t remain virtually unchanged until we get very close to $\partial V(\mathbf{z})$. The admissible set then collapses rather abruptly to a point corresponding to $\tilde{\mathbf{w}} \in \partial V(\mathbf{z})$.

The computations needed to make Figure 1 was done with the Advanpix Multiprecision Computing Toolbox for MATLAB (www.advanpix.com) using 100 digits of precision.

2.3 Interpolation

Let us assume now that the data $(\mathbf{z}, \mathbf{w}) \in \mathbb{C}^{2n}$ satisfies conditions of Theorem 2.4, i.e. $\mathbf{w} \in V(\mathbf{z})$. Our goal is to construct an interpolant $f \in \mathfrak{S}$, such that $f(z_j) = w_j$ for all $j = 1, \dots, n$. We begin with the case $n = 1$. According to Theorem 2.4, the necessary and sufficient condition for existence of such a function is $\Im(w_1) \geq 0$ and $\Im(z_1 w_1) \geq 0$. Of course, if $\Im(w_1) = 0$, then $w_1 \geq 0$, according to the second inequality, and $f(z) = w_1$ for all z . If $\Im(z_1 w_1) = 0$, then $zf(z)$ must be a real constant, and hence, according to the first inequality, $f = -\sigma/z$, where $\sigma = -z_1 w_1 \geq 0$. Let us now assume that

$$\Im(w_1) > 0, \quad \Im(z_1 w_1) > 0, \quad (2.14)$$

and characterize the set

$$\mathfrak{S}(z_1, w_1) = \{f \in \mathfrak{S} : f(z_1) = w_1\}.$$

We look for the answer in the same form as in the case of polynomials \mathcal{P} , where the set $\mathcal{P}(z_1, w_1)$ of all polynomials $p \in \mathcal{P}$ satisfying $p(z_1) = w_1$ can be described as

$$\mathcal{P}(z_1, w_1) = \{p(z) = (z - z_1)q(z) + w_1 : q \in \mathcal{P}\}.$$

Moreover, distinct polynomials $q \in \mathcal{P}$ correspond to distinct polynomials $p \in \mathcal{P}(z_1, w_1)$. By analogy with polynomials, we want to parametrize the set $\mathfrak{S}(z_1, w_1)$ by elements of \mathfrak{S} in the same fashion as $\mathcal{P}(z_1, w_1)$ is parametrized by elements of \mathcal{P} . Of course, we expect that the parametrization will be more complicated than in the case of polynomials.

It is easy to see that the general form expressing $f \in \mathfrak{S}(z_1, w_1)$ in terms of $g \in \mathfrak{S}$ must be a fractional-linear, or Möbius, transformation. According to Theorem 2.4 the set of all

admissible values $f(z)$ for $f \in \mathfrak{S}(z_1, w_1)$ is described by the inequalities

$$\det \mathbf{N}([z_1, z]; [w_1, f(z)]) = \frac{\Im(w_1)}{\Im(z_1)} \frac{\Im f(z)}{\Im(z)} - \left| \frac{f(z) - \overline{w_1}}{z - \overline{z_1}} \right|^2 \geq 0, \quad (2.15)$$

$$\det \mathbf{P}([z_1, z]; [w_1, f(z)]) = \frac{\Im(z_1 w_1)}{\Im(z_1)} \frac{\Im(z f(z))}{\Im(z)} - \left| \frac{z f(z) - \overline{z_1 w_1}}{z - \overline{z_1}} \right|^2 \geq 0. \quad (2.16)$$

Each of the two inequalities (2.15), (2.16) places $f(z)$ inside some closed disks $D_N(z_1, w_1, z)$ and $D_P(z_1, w_1, z)$, respectively. At the same time, Theorem 2.2 says that the Stieltjes class \mathfrak{S} itself is characterized by specifying the set of admissible values of $f(z)$: $f \in \mathfrak{S}$ if and only if $f(z)$ lies in the intersection of two closed half-planes $\overline{\mathbb{H}}_+ = \{w \in \mathbb{C} : \Im(w) \geq 0\}$ and $\mathbb{H}_z = \{w \in \mathbb{C} : \Im(zw) \geq 0\}$, for every $z \in \mathbb{H}_+$. This gives the idea of the desired parametrization of $\mathfrak{S}(z_1, w_1)$ by elements of \mathfrak{S} . For every $z \in \mathbb{H}_+$ there exists¹ a Möbius transformation

$$T_{z_1, w_1, z}(w) = \frac{L_{11}(z)w + L_{12}(z)}{L_{21}(z)w + L_{22}(z)}$$

that maps $\mathcal{A}(z; z_1, w_1) = D_N(z_1, w_1, z) \cap D_P(z_1, w_1, z)$ bijectively onto $\overline{\mathbb{H}}_+ \cap \mathbb{H}_z$. Since the descriptions of the disks $D_N(z_1, w_1, z)$ and $D_P(z_1, w_1, z)$ by formulas (2.15) and (2.16) are somewhat cumbersome we choose not to attempt computing $T_{z_1, w_1, z}(w)$ directly. Instead we exploit the simplicity of Stieltjes functions corresponding to the points on the boundary of the admissible region $\mathcal{A}(z; z_1, w_1)$. The idea is that while the set of functions in $\mathfrak{S}(z_1, w_1)$ is very large, if (2.14) is satisfied, it degenerates to a single point if any of the inequalities in (2.14) become equalities, as we have already discussed. The same holds for inequalities in (2.15), (2.16). If we have equality in (2.15), then there exist a nonzero vector $\xi = (\xi_1, \xi_2) \in \ker \mathbf{N}([z_1, z_2], [f(z_1), f(z_2)])$, where for convenience of notation we replaced z with z_2 . Using representation (2.2), we compute

$$\frac{f(z_j) - \overline{f(z_k)}}{z_j - \overline{z_k}} = \int_0^\infty \frac{d\sigma(t)}{(t - z_j)(t - \overline{z_k})}, \quad j, k = 1, 2.$$

Thus,

$$0 = (\mathbf{N}([z_1, z_2], [f(z_1), f(z_2)])\xi, \xi)_{\mathbb{C}^2} = \int_0^\infty \left| \frac{\xi_1}{t - z_1} + \frac{\xi_2}{t - z_2} \right|^2 d\sigma(t).$$

This means that there is a non-zero vector $(\xi_1, \xi_2) \in \mathbb{C}^2$, such that the function

$$\phi(t) = \frac{\xi_1}{t - z_1} + \frac{\xi_2}{t - z_2}$$

is identically zero on the support of σ . Since $z_1 \neq z_2$ we conclude that the support of σ must be a single point, and the corresponding Stieltjes function must have the form

$$f(z) = \gamma + \frac{\sigma}{t - z}. \quad (2.17)$$

¹Unique modulo $w \mapsto \alpha w$, $\alpha > 0$ and $w \mapsto -1/(zw)$.

Conversely, if the spectral measure of $f \in \mathfrak{S}(w_1, z_1)$ is supported on a single point, then we have equality in (2.15) for any $z \in \mathbb{H}_+$.

A similar analysis can be done for the case of equality in (2.16):

$$0 = (\mathbf{P}([z_1, z_2], [f(z_1), f(z_2)])\boldsymbol{\xi}, \boldsymbol{\xi})_{\mathbb{C}^2} = \gamma|\xi_1 + \xi_2|^2 + \int_0^\infty \left| \frac{\xi_1}{t - z_1} + \frac{\xi_2}{t - z_k} \right|^2 t d\sigma(t).$$

This equality implies that $f(z)$ must have either of two forms

$$f(z) = \gamma - \frac{\sigma_0}{z}, \text{ or } f(z) = -\frac{\sigma_0}{z} + \frac{\sigma_1}{t_1 - z}. \quad (2.18)$$

We can regard the first form of $f(z)$ as a limit of the second one when $\sigma_1 = \gamma t_1$, as $t_1 \rightarrow +\infty$.

Now, since the Möbius transformation $T_{z_1, w_1, z}(w)$ maps the boundary of $\mathcal{A}(z; z_1, w_1)$ onto the boundary of $\mathbb{H}_+ \cap \mathbb{H}_z$, the set

$$S_N(z_1, w_1) = \{f \in \mathfrak{S}(z_1, w_1) : \det \mathbf{N}([z_1, z_2], [f(z_1), f(z_2)]) = 0\},$$

consisting of functions (2.17) must be mapped by $T_{z_1, w_1, z}$ onto the set $\{g \in \mathfrak{S} : \Im(g(z)) = 0\}$, while the set

$$S_P(z_1, w_1) = \{f \in \mathfrak{S}(z_1, w_1) : \det \mathbf{P}([z_1, z_2], [f(z_1), f(z_2)]) = 0\},$$

consisting of functions (2.18) must be mapped by $T_{z_1, w_1, z}$ onto the set $\{g \in \mathfrak{S} : \Im(zg(z)) = 0\}$. This gives us the desired equations. If we write

$$g(z) = T_{z_1, w_1, z}(f(z)) = \frac{L_{11}(z)f(z) + L_{12}(z)}{f(z)L_{21}(z) + L_{22}(z)}, \quad (2.19)$$

then

$$f(z) = \frac{L_{22}(z)g(z) - L_{12}(z)}{L_{11}(z) - g(z)L_{21}(z)}. \quad (2.20)$$

Hence, the coefficients $L_{ij}(z)$ must satisfy the following properties: for any $\mu \geq 0$ the function $g(z) = \mu$ must be mapped into an element of $S_N(z_1, w_1)$, i.e. function of the form (2.17), while for any $\nu \geq 0$ the function $g(z) = -\nu/z$ must be mapped to an element of $S_P(z_1, w_1)$, i.e. function of the form (2.18). We therefore obtain the following system of equations for unknown coefficients $L_{ij}(z)$:

$$\begin{cases} \frac{L_{22}(z)\mu - L_{12}(z)}{L_{11}(z) - \mu L_{21}(z)} = \gamma(\mu) + \frac{\sigma(\mu)}{t(\mu) - z}, \\ -\frac{L_{22}(z)\nu + zL_{12}(z)}{zL_{11}(z) + \nu L_{21}(z)} = -\frac{\sigma_0(\nu)}{z} + \frac{\sigma_1(\nu)}{t_1(\nu) - z}, \\ \frac{L_{22}(z_1)\mu - L_{12}(z_1)}{L_{11}(z_1) - \mu L_{21}(z_1)} = w_1, \\ -\frac{L_{22}(z_1)\nu + z_1 L_{12}(z_1)}{z_1 L_{11}(z_1) + \nu L_{21}(z_1)} = w_1. \end{cases} \quad (2.21)$$

The last two equations are easy to solve, since the coefficients $L_{ij}(z)$ do not depend neither on μ nor on ν . Thus, we must require

$$\begin{cases} L_{11}(z_1)w_1 + L_{12}(z_1) = 0, \\ L_{21}(z_1)w_1 + L_{22}(z_1) = 0. \end{cases} \quad (2.22)$$

In order to solve the other two equations we first observe that equations

$$\begin{cases} \phi_N(z_1) = \gamma + \frac{\sigma}{t - z_1} = w_1, \\ \phi_P(z_1) = -\frac{\sigma_0}{z_1} + \frac{\sigma_1}{t_1 - z_1} = w_1 \end{cases} \quad (2.23)$$

determine two 1-parameter families of solutions $\phi_N(z; t)$ and $\phi_P(z; t_1)$, tracing the boundaries of D_N and D_P , respectively. Explicitly, we find

$$\begin{cases} \sigma = \frac{\Im(w_1)}{\Im(z_1)} |t - z_1|^2, \\ \gamma = \frac{\Im(z_1 w_1)}{\Im(z_1)} - t \frac{\Im(w_1)}{\Im(z_1)}, \\ \sigma_0 = \left(\frac{\Im(w_1)}{\Im(z_1)} - \frac{1}{t_1} \frac{\Im(z_1 w_1)}{\Im(z_1)} \right) |z_1|^2, \\ \sigma_1 = \frac{|t_1 - z_1|^2}{t_1} \frac{\Im(z_1 w_1)}{\Im(z_1)}. \end{cases} \quad (2.24)$$

This shows that for functions $\phi_N(z)$ and $\phi_P(z)$ to be in \mathfrak{S} it is necessary and sufficient that $t \in [0, t_*]$ and $t_1 \in [t_*, \infty]$, where

$$t_* = \frac{\Im(z_1 w_1)}{\Im(w_1)}.$$

We then see that when $t = t_1 = t_*$ we have

$$\phi_N(z) = \phi_P(z) = \frac{\sigma_*}{t_* - z}, \quad \sigma_* = \frac{\Im(w_1)}{\Im(z_1)} |t_* - z_1|^2 = \frac{|w_1|^2 \Im(z_1)}{\Im(w_1)}, \quad (2.25)$$

while when $t = 0$ and $t_1 = \infty$

$$\phi_N(z) = \phi_P(z) = \gamma_* - \frac{\sigma^*}{z}, \quad \gamma_* = \frac{\Im(z_1 w_1)}{\Im(z_1)}, \quad \sigma^* = \frac{|z_1|^2 \Im(w_1)}{\Im(z_1)}. \quad (2.26)$$

The correspondence between the two points of intersection of ∂D_N and ∂D_P and the two points of intersection of $\partial \mathbb{H}_+$ and $\partial \mathbb{H}_z$, characterized by $\mu = \nu = 0$ and $\mu = \nu = \infty$, respectively, is determined unambiguously by the orientation-preserving property of Möbius transformations. We conclude that the point $t = t_1 = t_*$ corresponds to $\mu = \nu = 0$, while the point $\mu = \nu = \infty$ corresponds to $t = 0, t_1 = \infty$. Hence, we have the equations

$$-\frac{L_{12}(z)}{L_{11}(z)} = \frac{\sigma_*}{t_* - z}, \quad -\frac{L_{22}(z)}{L_{21}(z)} = \gamma_* - \frac{\sigma^*}{z},$$

that permit us to eliminate L_{11} and L_{22} . Denoting

$$\Psi(z) = \frac{L_{21}(z)}{L_{12}(z)},$$

we obtain from the first equation in (2.21)

$$\frac{\left(\frac{\sigma^*}{z} - \gamma_*\right) \mu \Psi(z) - 1}{\frac{(z-t_*)}{\sigma_*} - \mu \Psi(z)} = \gamma(t(\mu)) + \frac{\sigma(t(\mu))}{t(\mu) - z}, \quad \gamma(t) = \frac{\gamma_*}{t_*}(t_* - t), \quad \sigma(t) = \frac{\gamma_*}{t_*}|t - z_1|^2$$

Solving this equation for Ψ (on Maple) we obtain that $\Psi(z)/z$ is a ratio of two quadratic polynomials in z with

$$\lim_{z \rightarrow \infty} \frac{\Psi(z)}{z} = \frac{t(\mu) - t_*}{\sigma_* \mu t(\mu)}.$$

Since $\Psi(z)$ does not depend on μ we conclude that there exists $\alpha \in \mathbb{R}$, such that

$$t(\mu) = \frac{t_*}{1 - \alpha \sigma_* \mu}. \quad (2.27)$$

Then, substituting (2.27) together with the parameter values

$$t_* = \frac{\Im(w_1)}{\Im(w_1)}, \quad \sigma_* = \frac{|w_1|^2 \Im(w_1)}{\Im(w_1)}, \quad \gamma_* = \frac{\Im(z_1 w_1)}{\Im(z_1)}, \quad \sigma^* = \frac{|z_1|^2 \Im(w_1)}{\Im(z_1)} \quad (2.28)$$

into the formula for $\Psi(z)$ in Maple we obtain that $\Psi(z) = \alpha z$. We can now go back and recover the formulas for all of the coefficients $L_{ij}(z)$:

$$\frac{L_{11}(z)}{L_{12}(z)} = \frac{z - t_*}{\sigma_*}, \quad \frac{L_{22}(z)}{L_{12}(z)} = \alpha(\sigma^* - \gamma_* z).$$

In this case it is easy to see that equations (2.22) will be satisfied. Thus, the desired Möbius transformation is given by

$$T_{z_1, w_1, z}(f(z)) = g(z) = \frac{1}{\alpha} \cdot \frac{(z - t_*)f(z) + \sigma_*}{zf(z) + \sigma^* - \gamma_* z}, \quad (2.29)$$

where the sign of α needs to be determined. It is easy to do when we examine the behavior of functions $f(z)$ and $g(z)$ at infinity. If we define

$$\gamma_g = \lim_{z \rightarrow \infty} g(z), \quad \gamma_f = \lim_{z \rightarrow \infty} f(z),$$

then, according to (2.29)

$$\gamma_g = \frac{\gamma_f}{\alpha(\gamma_f - \gamma_*)}, \quad \gamma_f = \frac{\alpha \gamma_* \gamma_g}{\alpha \gamma_g - 1}.$$

Since for any $g \in \mathfrak{S}$ we must get $f \in \mathfrak{S}(z_1, w_1)$ we conclude that we must have $\alpha < 0$. Since multiplication by $-\alpha > 0$ maps the intersection of the two half-planes \mathbb{H}_+ and \mathbb{H}_z onto itself, any choice of $\alpha < 0$ will produce a parametrization of $f \in \mathfrak{S}(z_1, w_1)$ by $g \in \mathfrak{S}$ via

$$f(z) = \frac{g(z)(\gamma_* z - \sigma^*) - \sigma_*}{zg(z) + z - t_*}, \quad (2.30)$$

where the coefficients are given in (2.28). Since our Möbius transformation maps $\mathcal{A}(z; z_1, w_1) = D_N(z_1, w_1, z) \cap D_P(z_1, w_1, z)$ onto the intersection of the two half-planes \mathbb{H}_+ and \mathbb{H}_z we conclude that $g \in \mathfrak{S}$ if and only if $f \in \mathfrak{S}(z_1, w_1)$. This gives the desired parametrization of $\mathfrak{S}(z_1, w_1)$:

$$\mathfrak{S}(z_1, w_1) = \left\{ \frac{g(z)(\gamma_* z - \sigma^*) - \sigma_*}{zg(z) + z - t_*} : g \in \mathfrak{S} \right\}, \quad (2.31)$$

provided inequalities (2.14) hold.

The parametrization (2.31) has other nice properties. At infinity we obtain

$$\gamma_f = \frac{\gamma_* \gamma_g}{\gamma_g + 1}. \quad (2.32)$$

This can be important in applications in the context of complex electromagnetic susceptibility functions, where the physically mandated assumption on the interpolant $f \in \mathfrak{S}$ is $\gamma_f = 0$. Formula (5.1) shows that $\gamma_f = 0$ if and only if $\gamma_g = 0$. This means that starting with $g(z) = 0$ and iterating formula (2.30) will always result in a decaying Stieltjes function $f(z)$.

Another nice feature of (2.30) is the degree-reduction property. To exhibit it let us solve (2.30) for $g(z)$:

$$g(z) = \frac{f(z)(t_* - z) - \sigma_*}{zf(z) + \sigma^* - \gamma_* z}. \quad (2.33)$$

LEMMA 2.5. *Suppose $f \in \mathfrak{S}(z_1, w_1)$ is a rational function of degree $n \geq 1$ in the sense that $f(z) = P_n(z)/Q_n(z)$, where the degree of Q_n is n , while the degree of P_n is either n or $n - 1$. Then $g(z)$, given by (2.33) is a rational function in \mathfrak{S} of degree at most $n - 1$.*

Proof. The essential feature of (2.33) is that all of its coefficients $L_{ij}(z)$ are linear in z . If $f(z) = P_n(z)/Q_n(z)$, then

$$L_{11}(z)f(z) + L_{12}(z) = \frac{L_{11}(z)P_n(z) + L_{12}(z)Q_n(z)}{Q_n(z)}.$$

Formulas (2.22) imply that the polynomial $L_{11}(z)P_n(z) + L_{12}(z)Q_n(z)$ will have a pair of complex conjugate roots z_1 and $\overline{z_1}$. We can therefore write

$$L_{11}(z)P_n(z) + L_{12}(z)Q_n(z) = (z - z_1)(z - \overline{z_1})T^+(z).$$

where the degree of $T^+(z)$ is at most $n - 1$. Similarly,

$$L_{21}(z)P_n(z) + L_{22}(z)Q_n(z) = (z - z_1)(z - \overline{z_1})T^-(z).$$

where the degree of $T^-(z)$ is at most $n - 1$. Hence,

$$g(z) = \frac{T^+(z)}{T^-(z)}$$

is a rational function of degree at most $n - 1$. □

The parametrization (2.31) of $\mathfrak{S}(z_1, w_1)$ by elements of \mathfrak{S} leads to the recursive interpolation algorithm. Given the data $\mathbf{w} \in V(\mathbf{z})$, $\mathbf{z} = (z_1, \dots, z_n)$ for n distinct points $\{z_1, \dots, z_n\} \subset \mathbb{H}_+$, we define the interpolant $f(z)$ by (2.30), where $g(z) \in \mathfrak{S}$ satisfies $n - 1$ constraints

$$g(z_j) = \frac{L_{11}(z_j)w_j + L_{12}(z_j)}{w_j L_{21}(z_j) + L_{22}(z_j)}, \quad j = 2, \dots, n, \quad (2.34)$$

provided

$$w_j L_{21}(z_j) + L_{22}(z_j) \neq 0, \quad j = 2, \dots, n.$$

In that case $f(z_j) = w_j$, $j = 2, \dots, n$, and

$$f(z_1) = \frac{L_{22}(z_1)g(z_1) - L_{12}(z_1)}{L_{11}(z_1) - g(z_1)L_{21}(z_1)}.$$

Using equations (2.22) we obtain

$$f(z_1) = \frac{-L_{21}(z_1)w_1g(z_1) + L_{11}(z_1)w_1}{L_{11}(z_1) - g(z_1)L_{21}(z_1)} = w_1,$$

provided $L_{11}(z_1) - g(z_1)L_{21}(z_1) \neq 0$. This condition is always satisfied, since linear functions $L_{ij}(z)$ are such that $f \in \mathfrak{S}$, for any $g \in \mathfrak{S}$. This requires that the denominator in (2.20) never vanishes when $z \in \mathbb{H}_+$.

In order to finish the analysis we need to consider the special case when there exists $k \in \{2, \dots, n\}$, such that

$$L_{22}(z_k) + w_k L_{21}(z_k) = 0. \quad (2.35)$$

In this case the corresponding relation (2.34) will be undefined. But in this case the 4 real equations

$$\begin{cases} L_{22}(z_k) + w_k L_{21}(z_k) = 0, \\ L_{22}(z_1) + w_1 L_{21}(z_1) = 0 \end{cases}$$

form a linear homogeneous system of equations with 4 real unknowns a_{21} , a_{22} , b_{21} , and b_{22} , where

$$L_{21}(z) = a_{21}z + b_{21}, \quad L_{22}(z) = a_{22}z + b_{22}.$$

Thus, the determinant of this system must vanish. Maple calculations show that this implies that $\det \mathbf{N} = 0$, where

$$\mathbf{N} = \begin{bmatrix} \frac{w_1 - \overline{w_1}}{z_1 - \overline{z_1}} & \frac{w_1 - \overline{w_k}}{z_1 - \overline{z_k}} \\ \frac{w_k - \overline{w_1}}{z_k - \overline{z_1}} & \frac{w_k - \overline{w_k}}{z_k - \overline{z_k}} \end{bmatrix}.$$

We have already proved that in this case the support of σ must be a single point. Thus, when (2.35) is satisfied we just return the rational function $\phi_N(z)$, given by (2.26). Indeed, (2.35) implies

$$w_k = \gamma_* - \frac{\sigma^*}{z_k} = \phi_N(z_k).$$

At the same time $\phi_N(z)$ also satisfies $\phi_N(z_1) = w_1$. It follows that $f(z) = \phi_N(z)$.

2.4 The least squares problem

For $\mathbf{w} \in \mathbb{C}^n$ there are two mutually exclusive logical possibilities. Either $\mathbf{w} \in V(\mathbf{z})$ or $\mathbf{w} \notin V(\mathbf{z})$. The former case, called the *interpolation problem* has been considered in the previous section. In the latter case, when there is no Stieltjes function f satisfying $\mathbf{w} = f(\mathbf{z})$, we want to solve the *least squares problem* (1.5), which can be also reformulated as

$$\Sigma(\mathbf{w}, \mathbf{z}) = \min_{\mathbf{p} \in V(\mathbf{z})} |\mathbf{p} - \mathbf{w}|. \quad (2.36)$$

The minimizer \mathbf{p}^* of (2.36) exists because $V(\mathbf{z})$ is a closed subset of \mathbb{C}^n . It is unique because $V(\mathbf{z})$ is convex. Moreover, since $\mathbf{w} \notin V(\mathbf{z})$, the minimizer \mathbf{p}^* must lie on the boundary of $V(\mathbf{z})$. In this case, the Nevanlinna-Pick theorem 2.4 says that there exists a unique Stieltjes function $f_* \in \mathfrak{S}$ satisfying $f_*(\mathbf{z}) = \mathbf{p}^*$.

Let us analyze the properties of this unique minimizer. Here we follow the analysis of Caprini [14], who derived the necessary and sufficient conditions for a minimizer in (2.36). Caprini's method is based on our ability to compute the effect of variations of γ and spectral measure σ in representation (2.2) on the functional we want to minimize. Suppose that

$$f_*(z) = \gamma + \int_0^\infty \frac{d\sigma(t)}{t - z}$$

is the minimizer in (1.5). Then $p_j^* = f_*(z_j)$ minimizes (2.36). Let

$$\tilde{f}(z) = \tilde{\gamma} + \int_0^\infty \frac{d\tilde{\sigma}(t)}{t - z} \quad (2.37)$$

be a competitor in (1.5), and let $\tilde{p}_j = \tilde{f}(z_j)$. The variation $\phi = \tilde{f} - f_*$ can then be written as

$$\phi(z) = \Delta\gamma + \int_0^\infty \frac{d\nu(t)}{t - z}, \quad \nu = \tilde{\sigma} - \sigma, \quad \Delta\gamma = \tilde{\gamma} - \gamma.$$

We then compute

$$|\tilde{\mathbf{p}} - \mathbf{w}|^2 - |\mathbf{p}^* - \mathbf{w}|^2 = |\tilde{\mathbf{p}} - \mathbf{p}^*|^2 + 2\Re(\mathbf{p}^* - \mathbf{w}, \tilde{\mathbf{p}} - \mathbf{p}^*).$$

Observing that

$$\tilde{p}_j - p_j^* = \Delta\gamma + \int_0^\infty \frac{d\nu(t)}{t - z_j},$$

we see that

$$\Re(\mathbf{p}^* - \mathbf{w}, \tilde{\mathbf{p}} - \mathbf{p}^*) = (\Delta\gamma) \Re \sum_{j=1}^n (p_j^* - w_j) + \int_0^\infty \Re \sum_{j=1}^n \frac{p_j^* - w_j}{t - \bar{z}_j} d\nu(t).$$

The real rational function

$$C(t) = \Re \sum_{j=1}^n \frac{p_j^* - w_j}{t - \bar{z}_j}, \quad t \geq 0, \quad (2.38)$$

which we will call *the Caprini function*, will play an essential role in our algorithm for solving the least squares problem (1.5).

In terms of the Caprini function we obtain

$$|\tilde{\mathbf{p}} - \mathbf{w}|^2 - |\mathbf{p}^* - \mathbf{w}|^2 = 2(\Delta\gamma) \lim_{t \rightarrow \infty} tC(t) + 2 \int_0^\infty C(t) d\nu(t) + |\tilde{\mathbf{p}} - \mathbf{p}^*|^2. \quad (2.39)$$

This formula permits us to formulate and prove Caprini's necessary and sufficient conditions for the minimizer in (2.36).

THEOREM 2.6. *Suppose that the minimum in (1.5) is nonzero, then the unique minimizer $f_* \in \mathfrak{S}$ is given by*

$$f_*(z) = \gamma + \sum_{j=1}^N \frac{\sigma_j}{t_j - z} \quad (2.40)$$

for some $\sigma_j > 0$, $t_j \geq 0$ and $\gamma \geq 0$. Moreover, f_* , given by (2.40) is the minimizer in (1.5) if and only if its Caprini function $C(t)$ is nonnegative and vanishes at $t = t_j$, $j = 1, \dots, N$, and "at infinity", in the sense that

$$\Re \sum_{j=1}^n (p_j^* - w_j) = \lim_{t \rightarrow \infty} tC(t) = 0, \quad (2.41)$$

provided $\gamma > 0$.

Proof. If $\gamma > 0$, then we can consider the competitor (2.37) with $\tilde{\sigma} = \sigma$. Formula (2.39) then implies that

$$2(\Delta\gamma) \lim_{t \rightarrow \infty} tC(t) + (\Delta\gamma)^2 > 0,$$

where $\Delta\gamma$ can be either positive or negative and can be chosen as small in absolute value as we want. This implies (2.41).

Next, suppose $t_0 \in [0, +\infty)$ is in the support of σ . For every $\epsilon > 0$ we define $I_\epsilon(t_0) = \{t \geq 0 : |t - t_0| < \epsilon\}$. Saying that t_0 is in the support of σ is equivalent to $m(t_0, \epsilon) = \sigma(I_\epsilon(t_0)) > 0$ for all $\epsilon > 0$. Then, there are two possibilities. Either

$$(i) \lim_{\epsilon \rightarrow 0} m(t_0, \epsilon) = 0, \text{ or}$$

$$(ii) \lim_{\epsilon \rightarrow 0} m(t_0, \epsilon) = \sigma_0 > 0$$

In case (i) we construct a competitor measure

$$\sigma_\epsilon(t) = \sigma(t) - \sigma|_{I_\epsilon(t_0)} + \theta m(t_0, \epsilon) \delta_{t_0}(t),$$

where $\theta > 0$ is an arbitrary constant. We then define

$$f_\epsilon(z) = \gamma + \int_0^\infty \frac{d\sigma_\epsilon(t)}{t - z}, \quad p_j^\epsilon = f_\epsilon(z_j). \quad (2.42)$$

Formula (2.39) then implies

$$\lim_{\epsilon \rightarrow 0} \frac{|\mathbf{p}^\epsilon - \mathbf{w}|^2 - |\mathbf{p}^* - \mathbf{w}|^2}{m(t_0, \epsilon)} = 2(\theta - 1)C(t_0).$$

If f_* is a minimizer, then we must have $(\theta - 1)C(t_0) \geq 0$ for all $\theta > 0$, which implies that $C(t_0) = 0$.

In the case (ii) we have $\sigma(\{t_0\}) = \sigma_0 > 0$. Then, for every $|\epsilon| < \sigma_0$ we construct a competitor measure

$$\sigma_\epsilon(t) = \sigma(t) + \epsilon \delta_{t_0}(t), \quad (2.43)$$

as well as the corresponding f_ϵ and \mathbf{p}^ϵ , given by (2.42). We then compute

$$\lim_{\epsilon \rightarrow 0} \frac{|\mathbf{p}^\epsilon - \mathbf{w}|^2 - |\mathbf{p}^* - \mathbf{w}|^2}{\epsilon} = 2C(t_0). \quad (2.44)$$

Since in this case ϵ can be both positive and negative we conclude that $C(t_0) = 0$.

Hence, we have shown that $C(t_0) = 0$ whenever $t_0 \in [0, +\infty)$ is in the support of the spectral measure σ of the minimizer f_* . It remains to observe that for any $t \in \mathbb{R}$

$$C(t) = \sum_{j=1}^n \left\{ \frac{p_j^* - w_j}{t - \bar{z}_j} + \frac{\overline{p_j^*} - \overline{w_j}}{t - z_j} \right\}.$$

Thus, $C(t)$ is a restriction to the real line of a rational function on the neighborhood of the real line in the complex t -plane. By assumption, $\mathbf{w} \notin V(\mathbf{z})$, and therefore $C(t)$ is not identically zero. In particular, $C(t)$ cannot have more than $2n - 1$ zeros. We conclude that the support of the spectral measure of the minimizer f_* must be finite:

$$\sigma(t) = \sum_{j=1}^N \sigma_j \delta_{t_j}(t), \quad N \leq 2n - 1.$$

and the minimizer must be a rational function.

Now let us consider the competitor (2.42) defined by (2.43), where $\epsilon > 0$ and $t_0 \notin \{t_1, \dots, t_N\}$. Formula (2.44) then implies that

$$\lim_{\epsilon \rightarrow 0^+} \frac{|\mathbf{p}^\epsilon - \mathbf{w}|^2 - |\mathbf{p}^* - \mathbf{w}|^2}{\epsilon} = 2C(t_0) \geq 0.$$

This proves that $C(t) \geq 0$ for all $t \geq 0$. The necessity of the stated properties of the Caprini function $C(t)$ is now established.

Sufficiency is a direct consequence of formula (2.39), since we can write

$$\nu(t) = \tilde{\sigma}(t) - \sigma(t) = \sum_{j=1}^N (\Delta\sigma_j) \delta_{t_j}(t) + \tilde{\nu}(t),$$

where $\tilde{\nu}(t)$ is a positive Radon measure without any point masses at $t = t_j$, $j = 1, \dots, N$. It is given by eliminating point masses of $\tilde{\sigma}$ at t_j , $j = 1, \dots, N$, if it has any:

$$\nu(t) = \tilde{\sigma}(t) - \sum_{j=1}^N \tilde{\sigma}(\{t_j\}) \delta_{t_j}(t).$$

We then compute, via formula (2.39), taking into account that $C(t_j) = 0$

$$|\tilde{\mathbf{p}} - \mathbf{w}|^2 - |\mathbf{p}^* - \mathbf{w}|^2 = 2(\Delta\gamma) \lim_{t \rightarrow \infty} tC(t) + 2 \int_0^\infty C(t) d\tilde{\nu}(t) + |\tilde{\mathbf{p}} - \mathbf{p}^*|^2 \geq 0,$$

since $C(t) \geq 0$. If $\Delta\gamma < 0$, then $\gamma = \tilde{\gamma} - \Delta\gamma > 0$, and therefore the first term on the right-hand side vanishes due to (2.41). \square

We observe that that if $t_j > 0$, then we must also have $C'(t_j) = 0$, since $t = t_j$ is a point of local minimum of $C(t)$. If we write formula (2.40) in the form

$$f_*(z) = \gamma - \frac{\sigma_0}{z} + \sum_{j=1}^N \frac{\sigma_j}{t_j - z}, \quad \gamma \geq 0, \sigma_0 \geq 0, t_j > 0, \sigma_j > 0, j = 1, \dots, N,$$

then we have exactly $2(N+1)$ equations for $2(N+1)$ unknowns $\gamma, \sigma_0, t_j, \sigma_j, j = 1, \dots, N$:

$$\gamma \lim_{t \rightarrow \infty} tC(t) = 0, \quad \sigma_0 C(0) = 0, \quad C(t_j) = 0, \quad C'(t_j) = 0, \quad j = 1, \dots, N. \quad (2.45)$$

Obviously, these equations do not enforce the nonnegativity of $C(t)$ and may very well be satisfied when some t_j are points of local maxima and $C(t)$ is not nonnegative. Hence, the equations should not really be regarded as equations for the minimizer. Instead the intended use of Theorem 2.6 is to provide the certificate of optimality of a purported solution of (2.36) by exhibiting the graph of $C(t)$ that shows that the necessary and sufficient conditions of optimality are satisfied. In fact, equations (2.45) are used in our algorithm to make the final adjustments when a near-optimal solution is obtained.

2.5 Analytic structure of the boundary of $V(\mathbf{z})$

The analytic structure of the feasible set $V(\mathbf{z})$ defined in (1.6) is well-understood. The set $V(\mathbf{z})$ is a closed convex cone in \mathbb{C}^n with non-empty interior $V^\circ(\mathbf{z})$, characterized by the inequalities $\mathbf{N}(\mathbf{w}) > 0$, $\mathbf{P}(\mathbf{w}) > 0$ in the sense of quadratic forms. The set

$$\mathfrak{S}(\mathbf{z}, \mathbf{w}) = \{f \in \mathfrak{S} : f(\mathbf{z}) = \mathbf{w}\}$$

is parametrized by elements of \mathfrak{S} via the recursive interpolation procedure described in Section 2.3. The function $f \in \mathfrak{S}(\mathbf{z}, \mathbf{w})$ corresponding to $0 \in \mathfrak{S}$ in such a parametrization has the form

$$f(z) = \sum_{j=1}^n \frac{\sigma_j}{t_j - z}, \quad \sigma_j > 0, \quad 0 < t_1 < \cdots < t_n.$$

with the list of parameters σ_j and t_j above, in one-to-one correspondence with points $\mathbf{w} = f(\mathbf{z})$ in $V^\circ(\mathbf{z})$ [40, 39].

By contrast with $V^\circ(\mathbf{z})$, each point on $\partial V(\mathbf{z})$ can be realized as a list of values of a unique Stieltjes function, which must necessarily be rational. In view of Theorem 2.4 the boundary of $V(\mathbf{z})$ can be naturally partitioned into two parts

$$\partial V^N(\mathbf{z}) = \{\mathbf{w} \in V(\mathbf{z}) : \det \mathbf{N}(\mathbf{w}) = 0\}, \quad \partial V^P(\mathbf{z}) = \{\mathbf{w} \in V(\mathbf{z}) : \det \mathbf{P}(\mathbf{w}) = 0\}.$$

We can think of them as two sides of a clam shell that meet along the rim

$$\partial V^{NP}(\mathbf{z}) = \{\mathbf{w} \in V(\mathbf{z}) : \det \mathbf{N}(\mathbf{w}) = 0, \det \mathbf{P}(\mathbf{w}) = 0\}.$$

Each point $\mathbf{w} \in \partial V^N(\mathbf{z})$ is attained by a unique rational function $f \in \mathfrak{S}_n^N$, where

$$\mathfrak{S}_n^N = \left\{ \gamma + \sum_{k=1}^{n-1} \frac{\sigma_k}{t_k - z} : \gamma \geq 0, \quad t_k \geq 0, \quad \sigma_k \geq 0 \right\}. \quad (2.46)$$

Similarly, each point $\mathbf{w} \in \partial V^P(\mathbf{z})$ is attained by a unique rational function $f \in \mathfrak{S}_n^P$. Unfortunately, a simple representation, like (2.46) of functions in \mathfrak{S}_n^P is not possible. This is because the parameter space $(\gamma, \boldsymbol{\sigma}, \mathbf{t})$ in (2.46) is non-compact, and it is an accident that the set \mathfrak{S}_n^N happens to be closed (in the space of holomorphic functions on $\mathbb{C} \setminus \mathbb{R}_+$). The most concise, but somewhat indirect description of \mathfrak{S}_n^P can be formulated using the “reflection” symmetry $\mathcal{R} : f \mapsto -1/(zf)$ of class \mathfrak{S} :

$$\mathfrak{S}_n^P = \mathcal{R}(\mathfrak{S}_n^N). \quad (2.47)$$

Implicitly \mathfrak{S}_n^P can be described as the closure of the set

$$\tilde{\mathfrak{S}}_n^P = \left\{ -\frac{\sigma_0}{z} + \sum_{k=1}^{n-1} \frac{\sigma_k}{t_k - z} : \sigma_0 \geq 0, \quad t_k \geq 0, \quad \sigma_k \geq 0 \right\} \quad (2.48)$$

with respect to uniform convergence on compact subsets of $\mathbb{C} \setminus \mathbb{R}_+$. Yet, the set \mathfrak{S}_n^P can also be described explicitly, as

$$\mathfrak{S}_n^P = \tilde{\mathfrak{S}}_n^P \cup \mathfrak{S}_{n-1}^N.$$

Similarly, each point $\mathbf{w} \in \partial V^{NP}(\mathbf{z})$ is attained by a unique rational function $f \in \mathfrak{S}_n^{NP}$, where \mathfrak{S}_n^{NP} can be described implicitly as the closure of

$$\tilde{\mathfrak{S}}_n^{NP} = \left\{ \sum_{k=1}^{n-1} \frac{\sigma_k}{t_k - z} : t_k \geq 0, \quad \sigma_k \geq 0 \right\}, \quad (2.49)$$

or explicitly, as

$$\mathfrak{S}_n^{NP} = \tilde{\mathfrak{S}}_n^{NP} \cup \mathfrak{S}_{n-1}^N.$$

If we define the evaluation operator $E_z : \mathfrak{S} \rightarrow \mathbb{C}^n$ by $E_z f = f(\mathbf{z})$, then we have both

$$V(\mathbf{z}) = E_z(\mathfrak{S}) \text{ and } V(\mathbf{z}) = E_z(\mathfrak{S}_{n+1}^{NP}).$$

Moreover, $E_z : \mathfrak{S}_{n+1}^{NP} \rightarrow V(\mathbf{z})$ is a bijection. The statements above are all consequences of the following classical theorem [28, 29]

THEOREM 2.7. *Suppose that $f \in \mathfrak{S}$ is a rational function. Then it can be written uniquely in the form*

$$f(z) = \gamma + \sum_{j=1}^n \frac{\sigma_j}{t_j - z}, \quad \gamma \geq 0, \sigma_j > 0, 0 \leq t_1 < t_2 < \dots < t_n, \quad (2.50)$$

where $n \geq 0$ is an integer. If $\gamma > 0$, then $f(z)$ has exactly n distinct real zeros $z = x_j$, $j = 1, \dots, n$, satisfying the interlacing property

$$0 \leq t_1 < x_1 < t_2 < x_2 < \dots < t_n < x_n < +\infty,$$

so that $f(z)$ can also be written as a product

$$f(z) = \gamma \prod_{j=1}^n \frac{z - x_j}{z - t_j}. \quad (2.51)$$

If $\gamma = 0$ and $n \geq 1$, then there are exactly $n - 1$ distinct real zeros $z = x_j$ and

$$f(z) = \frac{A}{t_n - z} \prod_{j=1}^{n-1} \frac{z - x_j}{z - t_j}, \quad A > 0, 0 \leq t_1 < x_1 < t_2 < \dots < x_{n-1} < t_n < +\infty. \quad (2.52)$$

3 A needle in a haystack

In Section 2 we have summarized a substantial body of existing knowledge about the Stieltjes class \mathfrak{S} and the closed convex cone $V(\mathbf{z})$. Can one harness this knowledge to devise an algorithm solving the least squares problem (2.36)? Surprisingly the answer is not apparent. What has been described so far is an interpolation algorithm for constructing functions $f(z)$, satisfying $f(z_j) = p_j^*$, once the solution \mathbf{p}^* of (2.36) has been found. In this section we take a closer look at the geometry of $V(\mathbf{z})$. Here will show that in effect, the set $V(\mathbf{z}) \subset \mathbb{C}^n$ has a very small (real) dimension compared to $2n$. The proverbial needle analogy is apt here. Even though the needle is a three-dimensional body, we can approximate it well by an interval of a straight line. To illustrate our point we return to our simple example (2.13). Figure 2 shows a two-dimensional cross-section of $V(\mathbf{z})$, where $\partial V^N(\mathbf{z})$ and $\partial V^P(\mathbf{z})$ parts of the boundary of $V(\mathbf{z})$ are shown in magenta and cyan and are on the left and the right side of $V(\mathbf{z})$, respectively. The origin in the figure is placed at \mathbf{w} in the interior of $V(\mathbf{z})$.

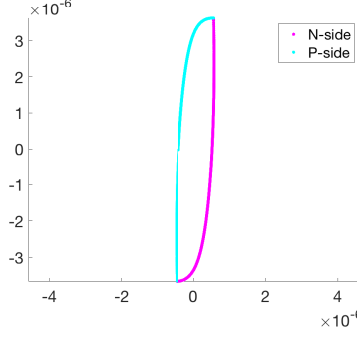


Figure 2: Two-dimensional cross-section of $V(\mathbf{z})$.

When we added a 2% noise to \mathbf{w} , the noisy data $\tilde{\mathbf{w}}$ would lie about 25,000 thicknesses of the cross-section away. If a surgical needle is the analogy, the scale in Figure 2 would put $\tilde{\mathbf{w}}$ about 25 meters away.

To see the dimensional degeneracy of $V(\mathbf{z})$ mathematically we recall that the rank-two displacement structure (2.11) and (2.12) of $\mathbf{N}(\mathbf{w})$ and $\mathbf{P}(\mathbf{w})$, respectively, implies that their eigenvalues decay exponentially fast [5]. Hence, numerically, these matrices will always have eigenvalues which are indistinguishable from 0 up to the floating point precision, when $n > 15$. Thus, numerically, all points in $V(\mathbf{z})$ will appear to lie on its boundary.

The crucial point here is that the dimensional degeneracy of the geometry of $V(\mathbf{z})$ handily defeats typical minimization algorithms that start with some initial guess $\mathbf{p}_0 \in \partial V(\mathbf{z})$ and choose the direction in which we want to travel “along” $\partial V(\mathbf{z})$ in order to make the distance to $\mathbf{w} \notin V(\mathbf{z})$ smaller. Indeed, even if we are travelling along one of the “long dimensions” of the needle, any tiny generic perturbation of the direction of travel will cause us to exit $V(\mathbf{z})$ after an extremely short distance. For example, when $n \approx 20$ our numerical experiments showed that we needed to perform 10^{10} steps to make even a barely noticeable change in the distance of $|\mathbf{p} - \mathbf{w}|$.

Graeme Milton [42] suggested that since $V(\mathbf{z})$ is a convex cone which is dimensionally degenerate it must effectively lie in a low-dimensional subspace of \mathbb{C}^n , in the same way as the needle whose point is at the origin, effectively lies in a one-dimensional subspace of \mathbb{R}^3 . In order to capture this low-dimensional subspace (or rather its orthogonal complement) we look for vectors $\boldsymbol{\xi} = (\xi_1, \dots, \xi_n) \in \mathbb{C}^n$, such that $|\boldsymbol{\xi}| = 1$ and $\Re(\mathbf{w}, \boldsymbol{\xi})$ is negligibly small for all $\mathbf{w} \in V(\mathbf{z})$ with $|\mathbf{w}| = 1$. Let us explore this idea.

Suppose $\gamma \geq 0$ and σ is the Stieltjes spectral measure. For given nodes $z_j \in \mathbb{H}_+$ we define

$$w_j[\sigma, \gamma] = \gamma + \int_0^\infty \frac{d\sigma(t)}{t - z_j}.$$

We estimate

$$|w_j[\sigma, \gamma]| \leq \gamma + \|\sigma\| \max_{t \geq 0} \left| \frac{t+1}{t - z_j} \right| \leq M(z_j)(\gamma + \|\sigma\|), \quad (3.1)$$

where

$$\|\sigma\| = \int_0^\infty \frac{d\sigma(t)}{t+1}, \quad M(z_j) = \max_{t \geq 0} \left| \frac{t+1}{t - z_j} \right|.$$

It is not hard to compute the constant $M(z)$ explicitly, when $\Im m(z) > 0$, using the theory of fractional-linear (Möbius) maps. We can also derive the reverse estimate from the formulas

$$\Im m(w_j) = \Im m(z_j) \int_0^\infty \frac{d\sigma(t)}{|t - z_j|^2},$$

and

$$\Re e(w_j) = \gamma + \int_0^\infty \frac{t - \Re e(z_j)}{|t - z_j|^2} d\sigma(t) = \gamma + \int_0^\infty \left| \frac{t+1}{t - z_j} \right|^2 \frac{d\sigma(t)}{t+1} - \frac{1 + \Re e(z_j)}{\Im m(z_j)} \Im m(w_j).$$

Denoting

$$m(z_j) = \min_{t \geq 0} \left| \frac{t+1}{t - z_j} \right| = \min \left\{ \frac{1}{|z_j|}, 1 \right\},$$

we obtain

$$m(z_j)(\gamma + \|\sigma\|) \leq \frac{\Im m(w_j z_j) + \Im m(w_j)}{\Im m(z_j)} \leq \frac{|z_j + 1|}{\Im m(z_j)} |w_j|. \quad (3.2)$$

Inequalities (3.1) and (3.2) imply that there exist constants $c(\mathbf{z})$ and $C(\mathbf{z})$, such that

$$c(\mathbf{z}) \|\mathbf{w}[\sigma, \gamma]\|_\infty \leq \gamma + \|\sigma\| \leq C(\mathbf{z}) \|\mathbf{w}[\sigma, \gamma]\|_\infty, \quad (3.3)$$

where

$$\|\mathbf{w}\|_\infty = \max_{1 \leq j \leq n} |w_j|, \quad c(\mathbf{z}) = \min_{1 \leq j \leq n} \frac{1}{M(z_j)}, \quad C(\mathbf{z}) = \min_{1 \leq j \leq n} \left\{ \frac{|z_j + 1|}{m(z_j) \Im m(z_j)} \right\}. \quad (3.4)$$

This means that $\gamma + \|\sigma\|$ and $\|\mathbf{w}\|_\infty$ are equivalent norms of $f \in \mathfrak{S}$, given by (2.2), provided $\mathbf{w} = f(\mathbf{z})$.

We recall that our goal is understand how the convex set

$$V_1(\mathbf{z}) = V(\mathbf{z}) \cap B(\mathbf{0}, 1)$$

would look like geometrically as a subset of the $2n$ -dimensional Euclidean space \mathbb{C}^n . We claim that this set, which is technically of full real dimension $2n$ is “very flat”. To quantify just how flat it is we look for unit vectors $\boldsymbol{\xi} \in \mathbb{C}^n$, such that $\Re e(\mathbf{w}, \boldsymbol{\xi})$ is very small for all $\mathbf{w} \in V_1(\mathbf{z})$. We compute

$$\Re e(\mathbf{w}, \boldsymbol{\xi}) = \Re e \left(\gamma S + \int_0^\infty \sum_{k=1}^n \frac{\xi_k}{t - \bar{z}_k} d\sigma(t) \right), \quad S = \sum_{k=1}^n \xi_k.$$

Since it is the measure $d\sigma(t)/(1+t)$ that is finite it will be convenient to rewrite the above formula as follows:

$$\Re e(\mathbf{w}, \boldsymbol{\xi}) = \Re e \left(\gamma S + \int_0^\infty (\psi[\boldsymbol{\xi}](t) + S) \frac{d\sigma(t)}{t+1} \right),$$

where

$$\psi[\boldsymbol{\xi}](t) = \sum_{k=1}^n \frac{\xi_k(\overline{z_k} + 1)}{t - \overline{z_k}}.$$

Thus,

$$|\Re(\mathbf{w}, \boldsymbol{\xi})| \leq (\gamma + \|\sigma\|)|\Re(S)| + \|\sigma\| \max_{t \geq 0} |\Re(\psi[\boldsymbol{\xi}](t))|.$$

Since $\theta[\boldsymbol{\xi}](t) = \Re(\psi[\boldsymbol{\xi}](t))$ is a complicated function of t whose maximum is impossible to compute directly we observe that both $\theta[\boldsymbol{\xi}]$ and $\theta'[\boldsymbol{\xi}]$ are in $L^2(0, +\infty)$ and use the inequality

$$\max_{t \geq 0} |\theta(t)|^2 \leq \|\theta\|_{1,2}^2 = \|\theta\|_{L^2(0,+\infty)}^2 + \|\theta'\|_{L^2(0,+\infty)}^2,$$

valid for all $\theta \in W^{1,2}(0, +\infty)$. The inequality is sharp. It becomes equality when $\theta(t) = e^{-t}$. Hence,

$$|\Re(\mathbf{w}, \boldsymbol{\xi})|^2 \leq 2(\gamma + \|\sigma\|)^2 (\Re(S)^2 + \|\theta[\boldsymbol{\xi}]\|_{1,2}^2) \leq 2C(\mathbf{z})^2 \|\mathbf{w}\|_\infty^2 \mathbf{Q}(\mathbf{z})[\boldsymbol{\xi}], \quad (3.5)$$

where

$$\mathbf{Q}(\mathbf{z})[\boldsymbol{\xi}] = \Re(S)^2 + \|\theta[\boldsymbol{\xi}]\|_{1,2}^2$$

is a positive definite real quadratic form in $\boldsymbol{\xi}$ and $C(\mathbf{z})$ is given in (3.4), in accordance with (3.2). Let $\lambda_1 > \lambda_2 > \dots > \lambda_{2n} > 0$ be the eigenvalues of $\mathbf{Q}(\mathbf{z})$. For each $\delta_m = C(\mathbf{z})\sqrt{2\lambda_{m+1}}$ taken as the “negligibility threshold”, we can regard m as the effective dimension of $V(\mathbf{z})$, since the $2n - m$ -dimensional span \mathcal{W}_m of all eigenvectors of $\mathbf{Q}(\mathbf{z})$ corresponding to eigenvalues λ_k , $k > m$ is effectively orthogonal to $V(\mathbf{z})$. Indeed, for any $\boldsymbol{\xi} \in \mathcal{W}_m$ and any $\mathbf{w} \in V_1(\mathbf{z})$ we have the inequality² $|\Re(\mathbf{w}, \boldsymbol{\xi})| \leq \delta_m$. For the example (2.13) the quadratic form is of full rank, its 40 eigenvalues decreasing from $\lambda_1 \approx 3.37 \cdot 10^8$ to $\lambda_{40} = 4.73 \cdot 10^{-5}$. If the number of data points increases to 40:

$$z_j = ie^{0.01+0.5j}, \quad j = 0, 1, \dots, 39.$$

Then numerical rank of the 80×80 matrix $\mathbf{Q}(\mathbf{z})$ is 56. It also remains 56 for the 100×100 matrix $\mathbf{Q}(\mathbf{z})$, corresponding to

$$z_j = ie^{0.01+0.4j}, \quad j = 0, 1, \dots, 49.$$

These results show that the theoretical bound (3.5) is fairly conservative and overestimates the perceived dimension of $V(\mathbf{z})$ quite a bit. A very different example (4.7) we discuss later gives $\text{rank}(\mathbf{Q}(\mathbf{z})) = 14$ for a 40×40 matrix $\mathbf{Q}(\mathbf{z})$.

The quadratic form $\mathbf{Q}(\mathbf{z})$ is not hard to compute explicitly using the residue formula

$$\int_0^\infty R(x)dx = - \sum_{r=1}^N \text{Res}[R(z) \ln(-z), z = p_r], \quad (3.6)$$

where $R(z)$ is a rational function with at least $1/|z|^2$ decay at infinity and poles p_r none of which lie on $[0, +\infty)$. Even with the exact formula for $\mathbf{Q}(\mathbf{z})$, the accurate computation of its eigenvalues requires many more digits of precision than the floating point allows even for $n = 20$. In our examples we have used the Advanpix Multiprecision Computing Toolbox for MATLAB (www.advanpix.com) using 200 digits of precision.

²Obviously, the estimate holds in a larger convex subset $V(\mathbf{z}) \cap B_\infty(\mathbf{0}, 1)$ of $V(\mathbf{z})$, where B_∞ denotes a ball in $\|\cdot\|_\infty$ norm of \mathbb{C}^n .

4 The least squares algorithm

In this section we describe the algorithm that solves the least squares problem (2.36), displays the graph of the Caprini function $C(t)$ certifying that the minimum in (2.36) has indeed been reached (see Theorem 2.6), and exhibit the “uncertainty band” where the least squares minimizer might belong for different realizations of the random noise in the data.

The first step in the algorithm is to replace $V(\mathbf{z})$ by a much simpler object: the positive span of an *ad-hoc basis* of $V(\mathbf{z})$.

Definition 4.1. *An ad-hoc basis of $V(\mathbf{z})$ is a finite set of positive spectral measures $\mathfrak{B} = \{\sigma_1, \dots, \sigma_N\}$, whereby $V(\mathbf{z})$ is replaced by*

$$V_{\mathfrak{B}}(\mathbf{z}) = \left\{ \mathbf{w} \in \mathbb{C}^n : w_j = x_0 + \sum_{\alpha=1}^N x_{\alpha} \phi_{\alpha}(z_j), \quad j = 1, \dots, n, \quad x_{\alpha} \geq 0, \quad \alpha = 0, 1, \dots, N \right\}, \quad (4.1)$$

where

$$\phi_{\alpha}(z) = \int_0^{\infty} \frac{d\sigma_{\alpha}(t)}{t - z}, \quad \alpha = 1, \dots, N.$$

The adjective “ad-hoc” indicates that our choice of the basis \mathfrak{B} is nothing more than an educated guess, and other choices could be at least as effective as our choice. The choice that appears to work very well consists of

- measures $\delta_{\tau}(t)$ —unit point mass at $t = \tau$, where τ is either the real or the imaginary part of one of z_j for some j ,
- measures $\chi_{[s_1, s_2]}(t)dt$, where s_1 and s_2 is either one of the τ s or a mid-point between adjacent τ s.

We will denote this construction of an ad-hoc basis by $\mathfrak{B}(\boldsymbol{\tau})$, where $\boldsymbol{\tau}$ stands for a list of τ ’s used in the above construction.

Imagining $V(\mathbf{z})$ as a needle explains why the choice of an ad-hoc basis can be fairly arbitrary. Indeed, selecting a point \mathbf{w}_0 at random inside a needle and replacing the needle with the ray $\{s\mathbf{w}_0 : s \geq 0\}$ gives a fairly accurate representation of the needle. The more accurately we want to approximate $V(\mathbf{z})$ the more important the choice of an ad-hoc basis becomes. Our choice above is just an attempt to tie the ad-hoc basis to the data in a somewhat natural and algorithmic fashion. Many existing algorithms (e.g. [9, 45]) make an effort of choosing such a basis, but in the absence of any rigorous approximation error analysis they also remain largely ad-hoc. In the new algorithm the ad-hoc basis is only needed as a stepping stone for the construction of a much better basis tailor-made for the specific experimental data.

Once the above ad-hoc basis has been chosen, we compute

$$p_j(\mathbf{x}) = x_0 + \sum_{\alpha=1}^N x_{\alpha} \phi_{\alpha}(z_j), \quad j = 1, \dots, n,$$

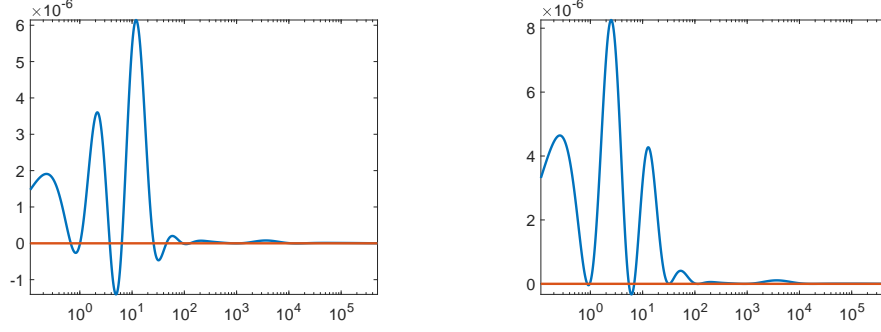


Figure 3: The Caprini function for the ad-hoc (left) and for the Caprini-augmented (right) bases projections.

by solving the nonnegative least squares problem

$$\min_{\mathbf{x} \geq 0} |\mathbf{p}(\mathbf{x}) - \mathbf{w}|^2. \quad (4.2)$$

The above least squares problem is solved by a well-established and widely implemented nonnegative least squares algorithm [32].

Naturally, we would like to know if our ad-hoc approximation to the solution of (2.36) is optimal. For illustration we once again turn to our simple example (2.13). We use the same noisy version $\tilde{\mathbf{w}}$ of \mathbf{w} as in the example of Figure 2. The optimality conditions described in Theorem 2.6 require the Caprini function $C(t)$ to be nonnegative and equal to zero on the support of the spectral measure. The graph of $C(t)$ shown in the left panel of Figure 3 suggests that we are not too far away from the true minimum, but are not there yet. Had we hit the minimum exactly, the local minima of $C(t)$ would also be both the global minima and the zeros of $C(t)$, and would comprise the support of the optimal spectral measure $\sigma(t)$. This observation leads to the next step in our algorithm: we add the points of local minima of $C(t)$ to the list of τ 's in our ad-hoc basis $\mathfrak{B}(\tau)$ and recompute $\mathbf{p}(\mathbf{x})$, solving (4.2) using the augmented ad-hoc basis $\mathfrak{B}(\tau_{\text{aug}})$ for $V(\mathbf{z})$. The Caprini function for the new approximation is shown in the right panel of Figure 3. We see both the substantial improvement and the fact that the new approximation \mathbf{p}^* is still not the true minimum in (2.36). We can repeat this step by adjoining the local minima of the improved Caprini function in the right panel of Figure 3 to the list of τ 's. The improvement after the second application of the augmentation of the ad hoc basis is significantly smaller, and more repetitions no longer lead to discernible improvements.

The next step in the algorithm is based on the author's experience trying to get the Caprini function to satisfy the sufficient conditions of optimality from Theorem 2.6 to within the computer precision. The Caprini function turns out to be extremely sensitive to even the tiniest deviations from the true optimum. The idea is to turn this curse into a blessing, by observing that noticeable changes in the optimality structure of $C(t)$ can be achieved by negligible changes not only in \mathbf{p}^* in (2.38), *but also in \mathbf{w} !* Observing that $\mathbf{p}^* \in V(\mathbf{z})$ by construction, we look for the *alternative data* $\tilde{\mathbf{w}}$ near \mathbf{w} , so that \mathbf{p}^* is a true minimizer in (2.36), where \mathbf{w} is replaced by $\tilde{\mathbf{w}}$, and where $\tilde{\mathbf{w}}$ is computed by requiring $C(t)$ to satisfy equations (2.45), where t_j are the locations of the local minima of the original $C(t)$. In

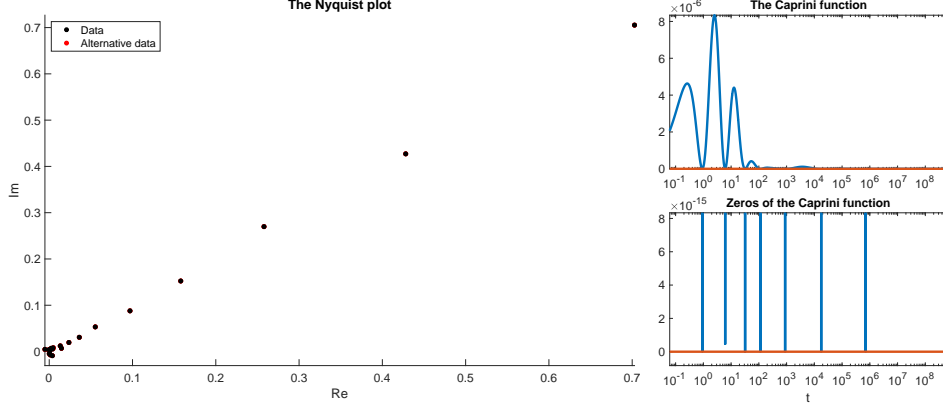


Figure 4: Achieving optimality for the “alternative data”.

other words we are looking for the vector $d\mathbf{w} \in \mathbb{C}^n$ of smallest norm, satisfying the following equations:

$$\begin{cases} \Re \sum_{j=1}^n \frac{dw_j}{(t_k - \bar{z}_j)^2} = 0, \\ \Re \sum_{j=1}^n \frac{dw_j}{t_k - \bar{z}_j} = C(t_k), \end{cases} \quad k = 1, \dots, N. \quad (4.3)$$

If we want to enforce $\gamma > 0$ condition we need to add the equation

$$\Re \sum_{j=1}^n dw_j = \Re \sum_{j=1}^n (p_j - w_j). \quad (4.4)$$

If $C(0) < 0$ for the original data we add $t = 0$ to the support of the spectral measure σ and require

$$\Re \sum_{j=1}^n \frac{dw_j}{\bar{z}_j} = -C(0). \quad (4.5)$$

Vector $d\mathbf{w}$ can then be computed using the least norm least squares solver (available from LAPACK, for example).

Our simulations show that the “alternative data” $\tilde{\mathbf{w}} = \mathbf{w} + d\mathbf{w}$ is indeed sufficiently close to the actual data to justify replacing one with the other. In other words, if we regard \mathbf{w} to be equal to \mathbf{p}^* plus random measurement errors, then $\tilde{\mathbf{w}}$ is also equal to \mathbf{p}^* plus a different realization of random measurement errors. At the same time the Caprini function for the alternative data $\tilde{\mathbf{w}}$ in Figure 4 shows that our formerly imperfect solution \mathbf{p}^* of (2.36) is now optimal to within the computer precision³. In Figure 4 we have plotted both \mathbf{w} and $\tilde{\mathbf{w}}$, and as expected, one cannot see any difference between them without zooming in on each data point.

On rare occasions during the algorithm testing the change from \mathbf{w} to $\tilde{\mathbf{w}}$ caused a point of local minimum $t = t_j$ of the original $C(t)$ to become a point of local maximum of the

³The bottom graph’s vertical scale is 10^{-9} times the top graph’s vertical scale

modified $C(t)$, while creating two new points of local minima to the right and to the left of t_j . If the new local minima are non-negligibly negative, then we update the list of local minima of $C(t)$ and apply the same “alternative data” procedure to $\tilde{\mathbf{w}}$, solving (4.3)–(4.5) again. In our numerical tests no more than two iterations of “data-fixing” was ever necessary to bring the graph of $C(t)$ into the desired shape.

In order to capture all local minima of $C(t)$ on $[0, +\infty)$ we observe that $C(t)$ will be a monotone function on $[T, +\infty)$ for sufficiently large T . Let us estimate the value of T . We will assume that $\gamma > 0$ and therefore

$$\Re \sum_{j=1}^n \delta_j = 0, \quad \delta_j = p_j - w_j.$$

In this case we can write $C'(t) = D_\infty(t) + O(t^{-4})$, as $t \rightarrow \infty$, where

$$D_\infty(t) = -\frac{2}{t^3} \Re \sum_{j=1}^n \delta_j \bar{z}_j.$$

Estimating $|C'(t) - D_\infty(t)|$, it is not hard to show that

$$|C'(t) - D_\infty(t)| < |D_\infty(t)|, \quad \forall t > T = (M_0 + 1) \max_{1 \leq j \leq n} |z_j|, \quad (4.6)$$

where

$$M_0 = \frac{2 \sum_{j=1}^n |\delta_j| |z_j|}{|\Re \sum_{j=1}^n \delta_j \bar{z}_j|}.$$

Inequality (4.6) shows that $C'(t)$ cannot be 0 when $t > T$. Hence, if we want to make sure that we missed no local minima of $C(t)$ we need to examine it only on the finite interval $[0, T]$.

In order to construct the function $f \in \mathfrak{S}$ satisfying $f(\mathbf{z}) = \mathbf{p}^*$ we run the recursive interpolation algorithm described in Section 2.3. In practice, even though matrices $\mathbf{N}(\mathbf{p}^*)$ and $\mathbf{P}(\mathbf{p}^*)$ have no numerically significant negative eigenvalues, feasibility gets lost after a number of iterations due to the amplification of round-off errors. This may happen even when n is as small as 10. When this occurs, we replace the currently infeasible data \mathbf{w} by its “projection” \mathbf{p}^* as described above and continue the recursion using the projected feasible data. The same mechanism that amplifies numerical noise during the forward recursion makes the results not very sensitive to small infidelities introduced by occasional projections onto the feasible set on some of the recursion steps. The outcome of such an “interpolation” algorithm, shown in Figure 5 is certifiably in \mathfrak{S} , even though it no longer interpolates the data exactly⁴. For this illustration we have taken a function

$$f(z) = 10 + \sum_{k=0}^9 \frac{|ak - 4 \ln 10|}{10^{-4} e^{ak} - z}, \quad a = \frac{8}{9} \ln 10,$$

⁴This would be visible if we magnified the neighborhood of some of the data points in Figure 5.

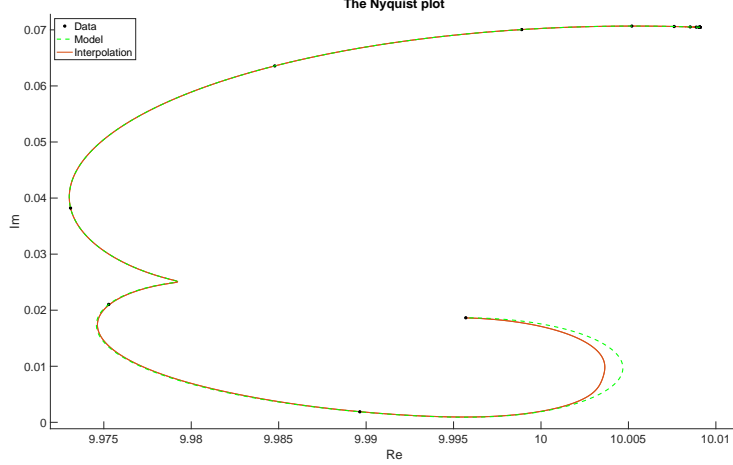


Figure 5: Data interpolation with intermediate projections onto the feasible set.

and used

$$z_j = 10^{-4}e^{bj} + 500i, \quad j = 0, 1, \dots, 19, \quad b = \frac{8}{19} \ln 10, \quad w_j = f(z_j). \quad (4.7)$$

A different way to obtain the solution of the least squares problem (1.5) is to use Theorem 2.6. In this approach we compute the locations t_k of local minima of the Caprini function corresponding to the “alternative data” $\tilde{\mathbf{w}}$ and $\mathbf{p}^* \in \partial V(\mathbf{z})$. We then solve, using the nonnegative least squares

$$\min_{\substack{\gamma \geq 0 \\ \sigma \geq 0}} \sum_{j=1}^n |F(z_j; \gamma, \boldsymbol{\sigma}) - p_j^*|^2, \quad F(z; \gamma, \boldsymbol{\sigma}) = \gamma + \sum_{k=1}^m \frac{\sigma_k}{t_k - z}.$$

While the recursive interpolation algorithm computes the values $f_*(z_\alpha)$ for *any* list $\{z_\alpha : \alpha = 1, \dots, N\} \subset \mathbb{H}_+$ without giving a formula for $f_* \in \mathfrak{S}$, the rational function $F(z; \gamma, \boldsymbol{\sigma})$ has an explicit spectral representation. In the numerical experiment corresponding to the model (2.13) and Figure 4 the values $p_j^* = f_*(z_j)$ are 0.6% closer to both \mathbf{w} and $\tilde{\mathbf{w}}$ than $q_j = F(z_j; \gamma, \boldsymbol{\sigma})$. In fact, the Caprini function plots in Figure 4 are based on \mathbf{p}^* and not on \mathbf{q} . In that respect we should regard $f_*(z_\alpha)$ to be the desired extrapolant solving the least squares problem (1.5).

The convenience of having a simple explicit formula for the extrapolant should not be underestimated. Unfortunately, if up to the numerical precision the data is feasible in the sense of satisfying conditions of Theorem 2.4, then the Caprini method cannot be used and only the values of the solution $f_* \in \mathfrak{S}$ of (1.5) at specified points are obtained via the recursion interpolation algorithm with occasional intermediate “projections” onto $V(\mathbf{z})$, whenever the data loses feasibility. In the next section we describe the algorithm for obtaining the spectral representation of f_* directly from the recursion interpolation algorithm from Section 2.3. In numerical experiments it seems to be superior to the indirect algorithm based on local minima of the Caprini function. It is also available for noiseless data, when the Caprini function cannot be constructed.

Finally, our algorithm tries to estimate the degree of uncertainty of the output. If we regard the discrepancies $w_j - f_*(z_j)$ as a random noise, then the fact that the measured values w_j are exactly what they are is in part an outcome of a random event. Simulating normal random noise with standard deviation

$$\rho^2 = \frac{1}{n} \sum_{j=1}^n |w_j - f_*(z_j)|^2$$

we produce other “realizations” of the error of measurement, each of which leads to its own least squares solution $f_*(z)$. Plotting these functions for 500 different realizations of the random noise gives one an idea of the degree to which we can trust the output of the algorithm. These potential realizations are shown in grey in Figures 6 and 7. While in [26, 27] we estimated the *worst case* error of extrapolation, these Monte-Carlo simulations are a simple and direct way to estimate the uncertainty for *specific data*.

5 Direct computation of spectral measure

Suppose that $\mathbf{p} \in V(\mathbf{z})$. The goal of this section is to describe an algorithm for computing the spectral representation (2.50) of the function $f \in \mathfrak{S}$ satisfying $f(\mathbf{z}) = \mathbf{p}$. The algorithm computes this representation recursively following the algorithm described in Section 2.3. It is based on the following theorem

THEOREM 5.1. *Suppose*

$$g(z) = \gamma_g - \frac{\sigma_0}{z} + \sum_{j=1}^n \frac{\sigma_j}{t_j - z}, \quad \gamma_g \geq 0, \sigma_0 \geq 0, \sigma_j > 0, 0 < t_1 < t_2 < \cdots < t_n,$$

Suppose $f(z)$ is given by (2.30). Then

$$f(z) = \gamma_f - \frac{\nu_0}{z} + \sum_{j=1}^{n+1} \frac{\nu_j}{\tau_j - z},$$

where

$$\gamma_f = \frac{\gamma_* \gamma_g}{\gamma_g + 1}, \quad \nu_0 = \frac{\sigma_0 \sigma^*}{\sigma_0 + t_*}, \quad (5.1)$$

and

$$0 < \tau_1 < t_1 < \tau_2 < t_2 < \cdots < t_n < \tau_{n+1}.$$

Proof. Formulas (5.1) are obtained by taking limits of $f(z)$ as $z \rightarrow \infty$ and $zf(z)$ as $z \rightarrow 0$ using formula (2.30). We have also shown in Section 2.3 that the degree of $f(z)$ is exactly 1 higher than $g(z)$. Proving that the intervals $(0, t_1), (t_1, t_2), \dots, (t_n, +\infty)$ contain at least one pole of $f(z)$ implies that these intervals must contain exactly one pole. The poles of $f(z)$ can only come either from poles of $g(z)$ or from the zeros of the denominator

$$\phi(z) = zg(z) + z - t_*.$$

It is easy to compute that

$$\lim_{z \rightarrow t_j} f(z) = \frac{\gamma_* t_j - \sigma^*}{t_j} \neq \infty.$$

Hence, only the zeros of $\phi(z)$ can be the positive poles of $f(z)$. The existence of zeros in the indicated intervals follows from the following observations

$$\lim_{x \rightarrow 0^+} \phi(x) = -\sigma_0 - t_* < 0, \quad \lim_{x \rightarrow t_j^\pm} \phi(x) = \mp \infty, \quad \lim_{x \rightarrow +\infty} \phi(x) = +\infty.$$

□

Once the intervals containing zeros of $\phi(x)$ are isolated, the zeros can be computed using the standard zero finding algorithm [10, 21]. We only need to derive the upper bound for the last pole τ_{n+1} . We observe that all functions

$$R_j(x) = \frac{x\sigma_j}{t_j - x}, \quad j = 1, \dots, n$$

are monotone increasing on $(t_n, +\infty)$. Thus, when $x \geq 2t_n$ we have

$$R_j(x) \geq -\frac{2t_n\sigma_j}{2t_n - t_j} \geq -2\sigma_j.$$

Therefore,

$$\phi(x) = (\gamma_g + 1)x - t_* - \sigma_0 + \sum_{j=1}^n R_j(x) \geq (\gamma_g + 1)x - t_* - 2 \sum_{j=0}^n \sigma_j.$$

We conclude that $\phi(x) > 0$ when $x > T_{\max}$, where

$$T_{\max} = \max \left\{ 2t_n, (\gamma_g + 1)^{-1} \left(t_* + 2 \sum_{j=0}^n \sigma_j \right) \right\}.$$

The spectral representation of $f(z)$ is then computed recursively with the explicit formula in the case when

$$g(z) = \gamma_g - \frac{\sigma_0}{z}.$$

Then formula (2.30) can be rewritten as

$$f(z) = f(z) = \frac{\gamma_* \gamma_g}{\gamma_g + 1} - \frac{\sigma_0 \sigma^*}{(\sigma_0 + t_*)z} + \frac{\nu_1}{\tau_1 - z}, \quad (5.2)$$

where

$$\tau_1 = \frac{\sigma_0 + t_*}{\gamma_g + 1}, \quad \nu_1 = \frac{\sigma^* \gamma_g + \sigma_* + \gamma_* \sigma_0}{\gamma_g + 1} - \frac{\gamma_* \gamma_g (\sigma_0 + t_*)}{(\gamma_g + 1)^2} - \frac{\sigma_0 \sigma^*}{\sigma_0 + t_*}.$$

In numerical experiments the values of $f_*(z)$ at specified points computed from the spectral representation of $f_*(z)$ are indistinguishable (graphically) from the values computed using the recursion algorithm from Section 2.3.

6 Case study: Electrochemical impedance spectroscopy

Electrochemistry studies electrical behavior of systems where the motion of charges occurs not only due to the applied electric field but also due to chemical reactions that occur on sometimes vastly different time scales. One of the key characteristics of such systems is the electrochemical impedance spectrum $Z(\omega)$ that has the meaning of resistance to an applied sinusoidal current. Combining the sine and cosine function into a complex exponential the steady response of such system to the current $I(t) = e^{i\omega t}$ is the voltage $U(t) = R(\omega)e^{i(\omega t + \phi(\omega))}$. The resistance $R(\omega)$ and the phase shift $\phi(\omega)$ are combined into a single complex valued function $Z(\omega) = R(\omega)e^{i\phi(\omega)}$ —the electrochemical impedance spectrum (EIS). The theory of electrochemical cells, including batteries, electrodes and electrolytes [3] says that $Z(\omega)$ has the spectral representation

$$Z(\omega) = R_\infty + \int_0^\infty \frac{d\sigma(\tau)}{1 + i\omega\tau}, \quad \int_0^\infty \frac{d\sigma(\tau)}{1 + \tau} < +\infty, \quad (6.1)$$

where σ is a positive Borel-regular measure on $[0, +\infty)$, called the distribution of relaxation times (DRT). This formula shows if $Z(\omega)$ is EIS, then $Z(\omega) = f(-i\omega)$ for some $f \in \mathfrak{S}$. It is also a continuum version of the complex impedance of an electrical circuit made of a series of Voigt elements, each being a resistor and a capacitor connected in parallel.

Definition 6.1. *A Voigt circuit is an electrical circuit made of finitely many resistors and capacitors.*

Theorem 6.2. *The complex impedance functions $Z(\omega)$ of Voigt circuits are in one-to-one correspondence with rational Stieltjes functions $\mathfrak{S}_{\mathcal{R}}$ via*

$$Z(\omega) = f(-i\omega), \quad f \in \mathfrak{S}_{\mathcal{R}}.$$

This theorem has long been known [22, 16, 17]. In electrochemistry there are several explicit EIS functions representing important electrochemical cells, each serving as a building block of more complex devices. The ideal capacitor's EIS $Z(\omega) = 1/(iC\omega)$ is often replaced by more realistic constant phase element (CPE) with

$$Z_{\text{CPE}}(\omega) = R/(i\tau\omega)^\phi, \quad \phi \in [0, 1].$$

Connecting it in parallel with a resistor gives the ZARC or Cole-Cole element

$$Z_{\text{ZARC}}(\omega) = \frac{R}{1 + (i\tau\omega)^\phi}, \quad \phi \in [0, 1].$$

A generalization of the ZARC element is the Havriliak-Negami element

$$Z_{\text{HN}}(\omega) = \frac{R}{(1 + (i\tau\omega)^\phi)^\psi}, \quad \phi \in [0, 1], \quad \psi \in [0, 1].$$

We test our algorithm on a double Havriliak-Negami element

$$Z_{\text{DHN}}(\omega) = R_\infty + \frac{R_0}{(1 + (i\tau_1\omega)^\phi)^\psi} + \frac{R_0}{(1 + (i\tau_2\omega)^\phi)^\psi}, \quad (6.2)$$

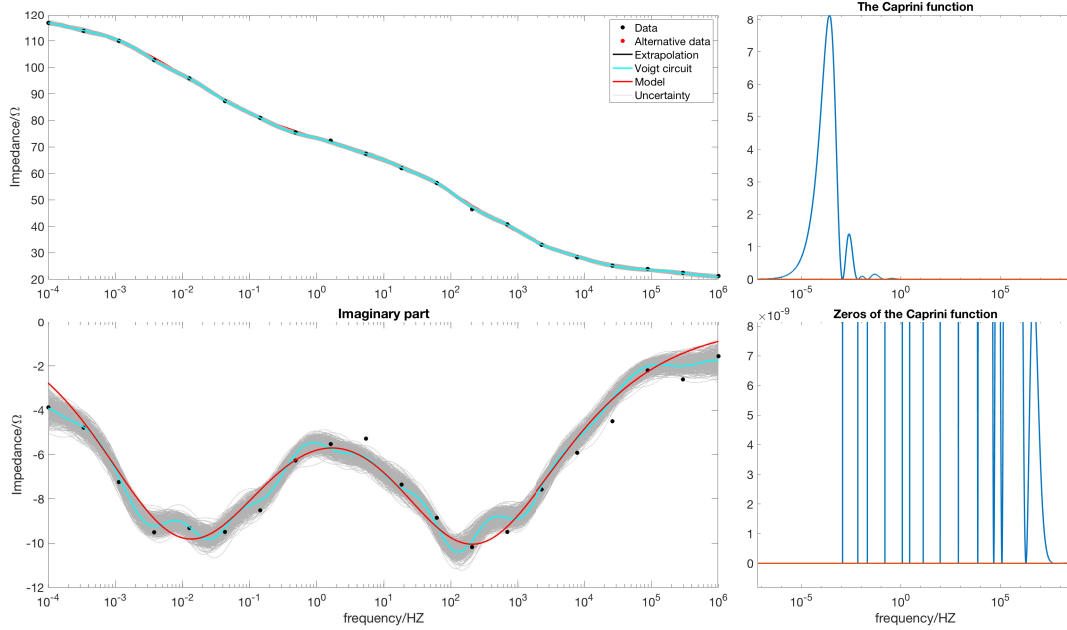


Figure 6: The output of the algorithm for a Voigt circuit.

where we chose

$$R_\infty = 20, R_0 = 50, \phi = 0.5, \psi = 0.8, \tau_1 = 20, \tau_2 = 0.001.$$

This element operates on two very different times scales (20 seconds and 1 millisecond) differing by 4 orders of magnitude.

The “experimental data” was produced by computing $Z_{\text{DHN}}(2\pi f)$ at 20 frequencies f_j equispaced on the logarithmic scale from $f_{\min} = 10^{-4}\text{Hz}$ to $f_{\max} = 10^6\text{Hz}$ and then polluting the exact values with 1% random noise on the relative scale. Figure 6 shows the result of the implementation of the algorithm. The real and imaginary parts of the exact EIS function (6.2) are shown in red. The imaginary part has exactly two local minima at $1/(2\pi\tau_1)$ and $1/(2\pi\tau_2)$. Since the random noise is complex-valued and $\Im(Z_{\text{DHN}})$ is 10 times smaller than $\Re(Z_{\text{DHN}})$, the relative size of the noise for the imaginary part is actually 10%. This is why the algorithm’s reconstructions seems to be better for the real part than for the imaginary part. While absolute errors of reconstruction for both the real and the imaginary parts are the same, the relative errors differ by a factor of 10.

There is no discernible difference between the actual and the “alternative data” for which the plots of the Caprini function at the global and local scales show certified optimality. The grey band indicates the uncertainty in the extrapolated black and cyan curves, which coincide almost to a floating point precision. The cyan curve is a plot of a rational function whose spectral measure is supported on 20 points. It is important to keep in mind that the results in Figure 6 look nice because we are “filling the gaps” between measurements. The situation changes if we try to extrapolate beyond the largest or the smallest frequency at which the impedance function has been measured. Figure 7 illustrates what happens with exactly the same “experimental data” when we ask the algorithm to reconstruct the EIS function on a

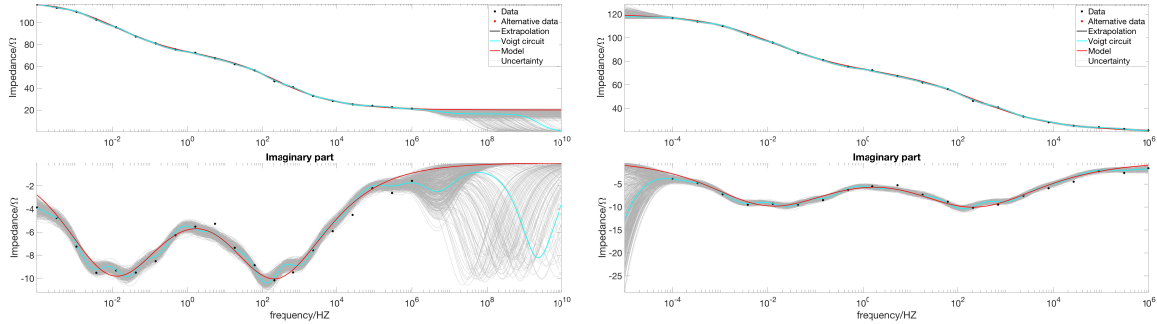


Figure 7: Extrapolation beyond the experimentally accessible frequency band.

larger frequency band. The uncertainty of reconstruction “explodes”, but our two methods of extrapolation: the recursive (black) and Caprini function-based spectral representation seem to agree. The uncertainty also explodes when we venture beyond the smallest frequency as well, while the consistency between the two methods of reconstruction is maintained. Both figures show a pronounced disagreement between the theoretical and the extrapolated curves away from the data, confirming that it is in general impossible to extrapolate sufficiently far away from the frequency band where the measurements have been made.

Acknowledgments. This material is based upon work supported by the National Science Foundation under Grant No. DMS-2005538.

References

- [1] A. Bard and L. Faulkner. *Electrochemical Methods; Fundamentals and Applications*. Wiley Interscience Publications, 2000.
- [2] E. Barsoukov and J. R. Macdonald, editors. *Impedance spectroscopy: theory, experiment, and applications*. Wiley Interscience Publications, 2nd edition, 2005.
- [3] E. Barsoukov and J. R. Macdonald, editors. *Impedance spectroscopy: theory, experiment, and applications*. John Wiley & Sons Inc., 2nd edition, 2005.
- [4] D. Batenkov, L. Demanet, and H. N. Mhaskar. Stable soft extrapolation of entire functions. *Inverse Problems*, 35(1):015011, 2019.
- [5] B. Beckermann and A. Townsend. On the Singular Values of Matrices with Displacement Structure. *SIAM J. Matrix Anal. Appl.*, 38(4):1227–1248, 2017.
- [6] D. J. Bergman. The dielectric constant of a composite material — A problem in classical physics. *Phys. Rep.*, 43:377–407, 1978.
- [7] R. Blankenbecler, M. L. Goldberger, S. W. MacDowell, and S. B. Treiman. Singularities of scattering amplitudes on unphysical sheets and their interpretation. *Phys. Rev.*, 123(2):692–699, Jul 1961.

- [8] B. A. Boukamp. A linear kronig-kramers transform test for immittance data validation. *Journal of the electrochemical society*, 142(6):1885, 1995.
- [9] B. A. Boukamp. Fourier transform distribution function of relaxation times; application and limitations. *Electrochimica acta*, 154:35–46, 2015.
- [10] R. P. Brent. *Algorithms for Minimization Without Derivatives*. Prentice-Hall, 1973.
- [11] O. Brune. Synthesis of a finite two-terminal network whose driving-point impedance is a prescribed function of frequency. *Journal of Mathematics and Physics*, 10(1-4):191–236, 1931.
- [12] I. Caprini. On the best representation of scattering data by analytic functions in L_2 -norm with positivity constraints. *Nuovo Cimento A (11)*, 21:236–248, 1974.
- [13] I. Caprini. Integral equations for the analytic extrapolation of scattering amplitudes with positivity constraints. *Nuovo Cimento A (11)*, 49(3):307–325, 1979.
- [14] I. Caprini. General method of using positivity in analytic continuations. *Rev. Roumaine Phys.*, 25(7):731–740, 1980.
- [15] I. Caprini. Constraints on physical amplitudes derived from a modified analytic interpolation problem. *J. Phys. A*, 14(6):1271–1279, 1981.
- [16] W. Cauer. Die Verwirklichung von Wechselstromwiderständen vorgeschriebener Frequenzabhängigkeit. *Archiv für Elektrotechnik*, 17(4):355–388, 1926.
- [17] W. Cauer. Über eine Klasse von Funktionen, die die Stieltjesschen Kettenbrüche als Sonderfall enthält. *Jahresbericht der Deutschen Mathematiker-Vereinigung*, 38:63–72, 1929.
- [18] E. Cherkaeva and K. M. Golden. Inverse bounds for microstructural parameters of composite media derived from complex permittivity measurements. *Waves Random Media*, 8(4):437–450, 1998.
- [19] L. Demanet and A. Townsend. Stable extrapolation of analytic functions. *Foundations of Computational Mathematics*, 19(2):297–331, 2018.
- [20] R. P. Feynman, R. B. Leighton, and M. Sands. *The Feynman lectures on physics. Vol. 2: Mainly electromagnetism and matter*. Addison-Wesley Publishing Co., Inc., Reading, Mass.-London, 1964.
- [21] G. E. Forsythe, M. A. Malcolm, and C. B. Moler. *Computer methods for mathematical computations*. Prentice-Hall, Inc., Englewood Cliffs, N.J., 1977.
- [22] R. M. Foster. Theorems regarding the driving-point impedance of two-mesh circuits. *The Bell System Technical Journal*, 3(4):651–685, 1924.

- [23] K. Golden and G. Papanicolaou. Bounds for effective parameters of multicomponent media by analytic continuation. *J. Statist. Phys.*, 40(5-6):655–667, 1985.
- [24] K. M. Golden. Bounds on the complex permittivity of sea ice. *J. Geophys. Res. (Oceans)*, 100(C7):699–711, 1995.
- [25] K. M. Golden and G. Papanicolaou. Bounds for effective parameters of heterogeneous media by analytic continuation. *Comm. Math. Phys.*, 90:473–491, 1983.
- [26] Y. Grabovsky and N. Hovsepyan. Explicit power laws in analytic continuation problems via reproducing kernel hilbert spaces. *Inverse Problems*, 36(3):035001, feb 2020.
- [27] Y. Grabovsky and N. Hovsepyan. Optimal error estimates for analytic continuation in the upper half-plane. *Comm Pure Appl Math*, 2021. to appear.
- [28] I. S. Kac and M. G. Krein. R-functions—analytic functions mapping the upper halfplane into itself. *Amer. Math. Soc. Transl.(2)*, 103(1):18, 1974.
- [29] I. V. Kac and M. G. Krein. *On the spectral functions of the string*, volume 103 of *Translations*. Amer Mathematical Society, 1974.
- [30] M. G. Krein and A. A. Nudelman. *The Markov Moment Problem and Extremal Problems*. Translation of Mathematical Monographs, 50. American Mathematical Society, Providence, RI, 1977.
- [31] L. D. Landau and E. M. Lifshitz. *Electrodynamics of continuous media*, volume 8. Pergamon, New York, 1960. Translated from the Russian by J. B. Sykes and J. S. Bell.
- [32] C. L. Lawson and R. J. Hanson. *Solving least squares problems*, volume 15 of *Classics in Applied Mathematics*. SIAM, 1995.
- [33] R. Lipton. Optimal inequalities for gradients of solutions of elliptic equations occurring in two-phase heat conductors. *SIAM Journal on Mathematical Analysis*, 32(5):1081–1093, 2001.
- [34] V. Lucarini, J. J. Saarinen, K.-E. Peiponen, and E. M. Vartiainen. *Kramers-Kronig relations in optical materials research*, volume 110. Springer Science & Business Media, 2005.
- [35] S. W. MacDowell. Analytic properties of partial amplitudes in meson-nucleon scattering. *Phys. Rev.*, 116(3):774–778, Nov 1959.
- [36] S. Mandelstam. Determination of the pion-nucleon scattering amplitude from dispersion relations and unitarity. general theory. *Phys. Rev.*, 112(4):1344–1360, Nov 1958.
- [37] J. V. Mantese, A. L. Micheli, D. F. Dungan, R. G. Geyer, J. Baker-Jarvis, and J. Grosvenor. Applicability of effective medium theory to ferroelectric/ferromagnetic composites with composition and frequency-dependent complex permittivities and permeabilities. *J. Appl. Phys.*, 79:1655–1660, 1996.

- [38] A. Mecozzi, C. Antonelli, and M. Shtaif. Kramers–kronig coherent receiver. *Optica*, 3(11):1220–1227, 2016.
- [39] G. W. Milton. Bounds on the complex permittivity of a two-component composite material. *J. Appl. Phys.*, 52:5286–5293, 1981.
- [40] G. W. Milton. Bounds on the transport and optical properties of a two-component composite material. *Journal of Applied Physics*, 52:5294–5304, 1981.
- [41] G. W. Milton. *Extending the Theory of Composites to Other Areas of Science*. Milton-Patton publishers, Salt Lake City, UT, USA, 2017.
- [42] G. W. Milton. Private communication, 2020.
- [43] J. Scully, D. Silverman, and M. Kendig, editors. *Electrochemical Impedance: Analysis and Interpretation*. ASTM, 1993.
- [44] L. N. Trefethen. Quantifying the ill-conditioning of analytic continuation. *BIT Numerical Mathematics*, 2020.
- [45] T. H. Wan, M. Saccoccio, C. Chen, and F. Ciucci. Influence of the discretization methods on the distribution of relaxation times deconvolution: implementing radial basis functions with drttools. *Electrochimica Acta*, 184:483–499, 2015.
- [46] M. Žic, S. Pereverzyev, V. Subotić, and S. Pereverzyev. Adaptive multi-parameter regularization approach to construct the distribution function of relaxation times. *GEM-International Journal on Geomathematics*, 11(1):2, 2020.